frontiers | Frontiers in Earth Science

TYPE Original Research
PUBLISHED 25 October 2022
DOI 10.3389/feart.2022.798387

OPEN ACCESS

EDITED BY
Stephen Self,
University of California, Berkeley,
United States

REVIEWED BY
Ilya Bindeman,
University of Oregon, United States
Francesca Forni,
University of Milan, Italy
Mark Stelten,
U.S. Geological Survey, United States

*CORRESPONDENCE
Guilherme A. R. Gualda,
g.gualda@vanderbilt.edu

SPECIALTY SECTION
This article was submitted to Volcanology,
a section of the journal
Frontiers in Earth Science

RECEIVED 20 October 2021
ACCEPTED 05 August 2022
PUBLISHED 25 October 2022

CITATION
Gualda GAR, Ghiorso MS, Hurst AA, Allen MC and Bradshaw RW (2022), A complex patchwork of magma bodies that fed the Bishop Tuff supereruption (Long Valley Caldera, CA, United States): Evidence from matrix glass major and trace-element compositions.
Front. Earth Sci. 10:798387.
doi: 10.3389/feart.2022.798387

A complex patchwork of magma bodies that fed the Bishop Tuff supereruption (Long Valley Caldera, CA, United States): Evidence from matrix glass major and trace-element compositions

Guilherme A. R. Gualda[1]*, Mark S. Ghiorso[2], Aaron A. Hurst[1,3], Madeline C. Allen[1] and Richard W. Bradshaw[1]

[1]Earth and Environmental Sciences, Vanderbilt University, Nashville, TN, United States, [2]OFM Research—West, Seattle, WA, United States, [3]United States Bureau of Reclamation, Denver, CO, United States

The geologic record reveals events in which enormous volumes (100–1000s of km^3) of magma were erupted in a matter of days to months. Yet, the architecture of magmatic systems that feed supereruptions can only be investigated through the study of ancient systems. For more than 40 years, the Bishop Tuff (Long Valley, California) has been the archetypal example of a single, zoned magma body that fed a supereruption. Early-erupted material is pyroxene-free and crystal poor (< 20 wt%), presumably erupted from the upper parts of the magma body; late-erupted material is orthopyroxene and clinopyroxene-bearing, commonly more crystal rich (up to 30 wt% crystals), and presumably tapped magma from the lower portions of the magma body. Fe-Ti oxide compositions suggest higher crystallization temperatures for late-erupted magmas (as high as 820°C) than for early-erupted magmas (as low as 700°C). Pressures derived from major-element compositions of glass inclusions were used to suggest an alternative model of lateral juxtaposition of two main magma bodies—each one feeding early-erupted and late-erupted units. Yet, this interpretation has proven controversial. We present a large dataset of matrix glass compositions for 227 pumice clasts that span the stratigraphy of the deposit. We calculate crystallization pressures based on major-element glass compositions using rhyolite-MELTS geobarometry and crystallization temperatures based on Zr in glass using zircon-saturation geothermometry. Additionally, we apply the same methods to 1,538 major-element and 615 trace-element analyses from a dataset from the literature. The results overwhelmingly demonstrate that the variations in crystallization temperature and pressure are not consistent with vertical stratification of a single magma body. All crystallization pressures and temperatures are very similar, with modes of ~150 MPa and ~730°C. Our results support lateral juxtaposition of three main magma bodies. Magmas represented by smaller stratigraphic units crystallized at similar pressures as the main bodies, which suggests coexistence of larger and smaller magma bodies at the time of

eruption. We compare our findings with results for other very large eruptions and supereruptions. We argue that supereruptions typically mobilize a complex patchwork of magma bodies that reside within specific levels of the crust. These eruptions reveal the architecture of the crust during moments of high abundance of eruptible magma, revealing crustal states that differ from what is inferred for magmatic systems currently present on Earth.

KEYWORDS

Bishop Tuff, supereruption, rhyolite, geothermobarometry, rhyolite-MELTS

Introduction

More than 40 years ago, Hildreth (1979) published a seminal study describing in detail the petrography, mineralogy, whole-rock and mineral geochemistry of pumice from the Bishop Tuff—the climatic eruption of the Long Valley Caldera, in California (Sheridan, 1965; Bailey et al., 1976; Hildreth, 2004), which erupted >600 km^3 of magma (Hildreth and Wilson, 2007) at around 765 ka (Andersen et al., 2017). The work by Hildreth (1979) was one of the first detailed studies of large rhyolitic ignimbrites, and the Bishop Tuff became a prime reference for our understanding of the structure of magma bodies that feed rhyolitic supereruptions. In his work, Hildreth (1979) describes a tantalizing range of temperatures derived from the equilibrium between the Fe-Ti oxides ilmenite and magnetite, as well as significant variations in mineral composition that correlate with the mineralogy of the studied pumice. These results were interpreted to represent progressive tapping of a vertically stratified magma body. Since then, the Bishop Tuff has been the archetypal example of a single, compositionally and thermally vertically stratified magma body that fed a supereruption. Significant work has followed this early study (Halliday et al., 1984; Hildreth and Mahood, 1986; Wallace et al., 1995, 1999; Wilson and Hildreth, 1997; Anderson et al., 2000; Reid and Coath, 2000; Peppard et al., 2001; Bindeman and Valley, 2002; Gualda et al., 2004; Hildreth, 2004; Simon and Reid, 2005; Hildreth and Wilson, 2007; Wark et al., 2007; Reid et al., 2011; Pamukcu et al., 2012, 2016; Evans and Bachmann, 2013; Roberge et al., 2013; Chamberlain et al., 2014a, 2014b, 2015; Gualda and Sutton, 2016; Jolles and Lange, 2019), and the idea of a single stratified magma body has remained unchallenged—until relatively recently (Gualda et al., 2012; Gualda and Ghiorso, 2013a).

Against the backdrop of the work on the Bishop Tuff, evidence in the literature has been accumulating that many very large to supereruption deposits were formed by eruption of multiple large to very large magma bodies, instead of deriving from a single giant magma body (Gravley et al., 2007; Cooper et al., 2012; Bégué et al., 2014a; Cashman and Giordano, 2014; Pearce et al., 2019). In this alternative scenario, multiple magma bodies coexist at the same time and they are tapped by the same eruption; however, they do not necessarily interact chemically, and the compositional variations observed are discretized, rather than continuously variable. The crustal configuration resulting from the presence of multiple contemporaneous magma bodies is rather different from that invoked by the traditional view of a single stratified magma body—the construction, stability, and longevity of a system comprising multiple magma bodies is potentially significantly distinct from that of a single larger mechanical and thermal anomaly within the crust (Jellinek and DePaolo, 2003).

Gualda and Ghiorso (2013a) suggest that the Bishop Tuff could have been erupted from at least two laterally juxtaposed magma bodies. The evidence comes 1) from glass geothermobarometry for a dataset of glass inclusion compositions from the literature (Wallace et al., 1995, 1999; Anderson et al., 2000), which suggests similar crystallization pressures and temperatures for early and late-erupted pumice; and 2) from reinterpretation of some of the mineral composition data from Hildreth (1979) and the glass compositional data from Wallace et al. (1999) and Anderson et al. (2000), which suggest discrete compositional ranges for early and late-erupted pumice. However, this alternative view of the structure of the Bishop Tuff magmatic system has encountered significant resistance in more recent work (Evans and Bachmann, 2013; Chamberlain et al., 2014a, 2014b, 2015; Evans et al., 2016; Jolles and Lange, 2019). A significant source of criticism seems to stem from the nature of the set of compositions used by Gualda and Ghiorso (2013a), which encompasses samples purposefully selected for the study of volatiles in glass inclusions (Wallace et al., 1999; Anderson et al., 2000), rather than being a comprehensive set of samples that spans the stratigraphy of the deposit in detail. Further criticism derives from the conflicting record of temperatures retrieved by different methods (Hildreth, 1979; Hildreth and Wilson, 2007; Gualda et al., 2012; Gualda and Ghiorso, 2013a; Evans and Bachmann, 2013; Ghiorso and Gualda, 2015; Evans et al., 2016; Jolles and Lange, 2019).

In the context of understanding the architecture of magmatic systems (Annen et al., 2015; Cashman et al., 2017), it becomes important to resolve the controversy surrounding the Bishop Tuff magma body. Is the Bishop Tuff an end-member case of the more traditional view in which a single zoned magma body fed a supereruption—what Gualda and Ghiorso (2013a) dubbed the

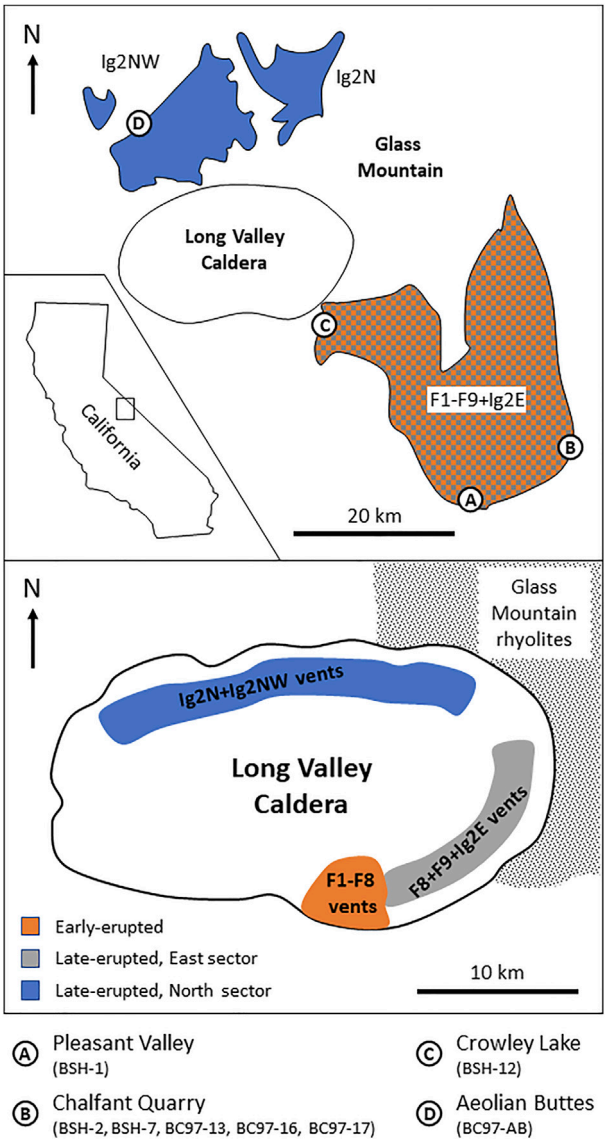

FIGURE 1
Simplified map of the Bishop Tuff showing sampling localities within the deposit (Vanderbilt dataset only). Top diagram shows location of the Long Valley Caldera and the distribution of early-erupted (orange), East-sector late-erupted (gray), and North-sector late-erupted (blue) deposits. Early-erupted deposits underlie East-sector late-erupted deposits, which is shown by the cross-hatched pattern. Localities where studied pumice clasts were collected are indicated. Bottom diagram shows the inferred distribution of vents that led to deposition of the Bishop Tuff, with the same color-coding as in top diagram. Note the location of the Glass Mountain volcanic edifice, which limited the deposition of the Bishop Tuff in that region. Figures adapted from Wilson and Hildreth (1997).

"Standard Model"? Or is the Bishop Tuff the result of tapping of multiple magma bodies during a supereruption, as it appears to be the case in other examples (the model favored by Gualda and Ghiorso, 2013a)?

In order to address this question, and to overcome the limitations of the sample set used by Gualda and Ghiorso (2013a), we present here an extensive dataset of matrix glass compositions for pumice clasts that span the stratigraphy of the deposit. We also take advantage of a comparable and complementary set of matrix glass compositions published by Chamberlain et al. (2015). We use major-element compositions to calculate crystallization pressures using the rhyolite-MELTS geobarometer (Gualda et al., 2012; Gualda and Ghiorso, 2014); and we use zircon-saturation geothermometry to calculate crystallization temperatures (Watson and Harrison, 1983; Hanchar and Watson, 2003; Boehnke et al., 2013). The present study uses an approach that is similar to that of Gualda and Ghiorso (2013a), but with a much larger sample set that better represents the stratigraphy and the overall compositional variability observed in the Bishop Tuff. Further, we use multivariate analysis to identify compositional groups that might indicate the involvement of discrete magma bodies. In this regard, the present study goes beyond the work of Gualda and Ghiorso (2013a), in providing a more quantitative assessment of the compositional variability observed in pumice from the Bishop Tuff. The results presented allow us to distinguish between the two contrasting models for the architecture of the Bishop Tuff magmatic system, with implications for the understanding of the architecture of supereruption-forming magmatic systems.

Materials and methods

In this study, we present geothermobarometric results using two datasets of matrix glass compositions from pumice clasts from the Bishop Tuff: 1) a dataset of major and trace-element compositions obtained at Vanderbilt University as part of this study (hereafter "Vanderbilt dataset"); and 2) a dataset of major and trace-element compositions from Chamberlain et al. (2015) (hereafter "Chamberlain dataset"). We describe below sampling and analyses used to generate the Vanderbilt dataset, and we give some general characteristics of the Chamberlain dataset.

Sampling

Samples that compose the Vanderbilt dataset come from four localities within the Bishop Tuff deposit (Figure 1; Table 1): (A) Pleasant Valley (BSH-1 locality), in the southern end of the deposit, where samples from units F7, F8, F9, and Ig2Ea were collected (nomenclature according to Wilson and Hildreth, 1997); (B) Chalfant Quarry (BSH-2, BSH-7, BC97-13, BC97-16, and BC97-17), in the southeastern end of the deposit, where samples from units F5, F6, F7, Ig1Eb, F8, F9, and Ig2Ea were collected; (C) Lake Crowley (BSH-12), near the eastern rim of the Long Valley caldera, where samples from units F5, F6, and Ig1Ea

TABLE 1 Outcrop locations and units sampled for pumice clasts used in this study (Vanderbilt dataset only).

Outcrop	Units sampled	Locality	Year	Latitude	Longitude
BSH-1[a]	F6, F7, Ig1Eb, F8, F9, Ig2Ea	Pleasant View	2003	37°24′39.89″N	118°30′52.43″W
BSH-2[a]	F6, F7, Ig1Eb, F8, F9, Ig2Ea	Chalfant Quarry	2003	37°27′36.35″N	118°22′0.96″W
BSH-7[b]	F5, F9	Chalfant Quarry	2015	37°27′36.35″N	118°22′0.96″W
BSH-12	Ig1Ea, F6, Ig1Eb	Crowley Lake	2016	37°36′12.76″N	118°43′14.98″W
BC97-13[c]	F8, F9	Chalfant Quarry	1997	See Gualda et al. (2004)	
BC97-16[c]	F7	Chalfant Quarry	1997	See Gualda et al. (2004)	
BC97-17[c]	Ig2Ea	Chalfant Quarry	1997	See Gualda et al. (2004)	
BC97-AB[c]	Ig2NWb	Aeolian Buttes	1997	See Pamukcu et al. (2012)	

[a]No GPS location from 2003 campaign; same locality visited in 2015
[b]Same locality as BSH-2, revisited in 2015
[c]Samples collected by Alfred T. anderson jr.

were collected; (D) Aeolian Buttes (BC97-AB), in the northwestern part of the deposit, where samples from unit Ig2NW were collected. Chalfant Quarry and Aeolian Buttes localities were the focus of prior studies by our group (Gualda et al., 2004; Gualda, 2006; Gualda and Rivers, 2006; Gualda and Anderson, 2007; Gualda and Ghiorso, 2007; Gualda et al., 2012; Pamukcu et al., 2012, 2015a), while this is the first time we study the materials from Pleasant Valley and Lake Crowley. Samples labelled BC97 are from a collection from Alfred T. Anderson Jr, while the other samples were collected by Gualda in field trips in 2003, 2015, and 2016 (see Table 1).

In combination, our samples span fall units F5-F9, including samples from both flow units intercalated within the fall units (Ig1Ea and Ig1Eb), as well as samples from Ig2Ea and Ig2NW. As such, our samples cover much of the stratigraphy of the Bishop Tuff. It is interesting to note that our sample set is characterized by a majority of samples from the fall units. In contrast, the sample set of Chamberlain et al. (2015) has a preponderance of samples from the various flow deposits, and it also includes samples from fall units F1-F4. The combined datasets span the entire stratigraphy of the deposit, including some of the smaller and less typical deposits included in the Chamberlain dataset.

Following on the work of Hildreth (1979) and Wilson and Hildreth (1997), we divide our samples of the Bishop Tuff into two main groups of units (see Figure 1): 1) The early-erupted Bishop Tuff comprises the lower units of the stratigraphy; its pumice is characteristically crystal poor and lacks pyroxenes, and it forms deposits that lack fragments of the nearby Glass Mountain volcanics; 2) the late-erupted Bishop Tuff, whose pumice is somewhat more variable in crystal contents (see Pamukcu et al., 2012), contains both orthopyroxene and clinopyroxene, includes Glass Mountain fragments among the lithics, and forms the upper units of the deposit. We further subdivide the late-erupted Bishop Tuff into two subgroups (see Figure 1): 1) units that appear to the east and south of the caldera (hereafter "East sector"); and 2) units that appear to the north and northwest of the caldera (hereafter "North sector"). In this context, our samples from units F5-F7, Ig1Ea, and Ig1Eb are from the early-erupted Bishop Tuff; samples from units F8-F9 and Ig2E are from the East sector of the late-erupted Bishop Tuff; and samples from unit Ig2NW are from the North sector of the late-erupted Bishop Tuff. We similarly divide the samples from the Chamberlain dataset into these three groups.

Sample preparation

A total of 227 pumice clasts were used in the Vanderbilt dataset (127 from early-erupted units; 81 from East-sector late-erupted units; and 19 from North-sector late-erupted units). Each pumice clast was cleaned with a stiff brush to remove any adhering extraneous material. Small fragments of each pumice clast were mounted in epoxy, ground to expose the interior of the fragment, and polished down to 1 μm grit prior to analysis. Each mount was photographed using a light microscope and Carbon-coated prior to analytical work.

Major-element analysis

Major-element compositions were determined via quantitative energy-dispersive x-ray (EDX) analysis using an Oxford X-max 50 mm2 solid-state EDX detector attached to a Tescan Vega 3 LM variable-pressure scanning electron microscope (SEM) with a LaB_6 electron source installed at the Department of Earth and Environmental Sciences, Vanderbilt University. We used high-vacuum with an accelerating voltage of 15 kV, working distance of 15 mm, and a beam intensity of 18–19, which results in an absorbed current of ~2 nA. Analysis was performed with the Oxford program AZtec using factory standards, process time 4, and dead time optimized to 50–60% (so as to maximize x-ray output count-rate to about 20k-25k counts per second). Live acquisition times were 20 s per area, which provides a good compromise between minimizing beam

damage to the sample (critical when analyzing rhyolitic glass) and obtaining sufficient counts for minor elements such as Ti and Mg. Small rectangular areas (10 s of μm across) were selected for analysis (also to minimize beam damage), being careful to avoid crystals and epoxy.

A total of 10–20 analyses were obtained per pumice clast, which allowed identification of outliers due to alteration and the presence of inclusions; this also allows averaging of several analyses, which yields better results without additional beam damage.

Quality of the results was monitored by performing analyses of the RGM-1 standard—which we fused in house at atmospheric pressure—as a secondary standard in every analytical session. As demonstrated by Pamukcu et al. (2015a) and Pamukcu et al. (2021), analysis using our SEM-EDX setup yields the expected compositions for RGM-1 with similar or superior uncertainties to those obtained with the electron probe for major elements.

Trace-element analysis

Trace-element matrix glass compositions were obtained using a Photon Machine Excite 193 nm excimer laser ablation (LA) system attached to a ThermoFisher iCAP Qc quadrupole inductively coupled plasma mass spectrometer (ICPMS) installed at Vanderbilt University. We used spot sizes of 50 μm, pulse rate of 10 Hz for 25 s, with He as carrier gas at a flow rate of 0.72 L/min. A total of 30 analytes were measured, and data acquisition in the ICPMS system started 20 s prior to ablation of the sample by the laser. Si was used as an internal standard, with values for SiO_2 obtained by SEM-EDX. Reference material NIST-610 (or NIST-612) was used for calibration, and NIST-612 (or NIST-610), NIST-614, and RGM-1 were treated as unknowns and evaluated as secondary standards. Data were reduced using the software Glitter (Griffin et al., 2008). Results suggest uncertainties of no more than 10% for most elements reported here (based on external reproducibility of secondary standards, at 1-sigma level).

Projection of glass analyses on the haplogranitic ternary

Following Gualda et al. (2012) and Gualda and Ghiorso (2013b), we project all matrix glass compositions on the haplogranitic (quartz-albite-orthoclase) ternary, using the projection scheme of Blundy and Cashman (2001) to correct for the presence of anorthite in natural compositions. Given that the projection scheme was developed for strictly metaluminous compositions (see Blundy and Cashman, 2001), we exclude compositions with normative corundum greater than 0.5 (i.e. more strongly peraluminous; those with alumina saturation index [ASI = $\{Al_2O_3/(CaO+N_2O+K_2O)\}_{molecular}$] >~ 1.05).

Rhyolite-MELTS geobarometry

We use rhyolite-MELTS (Gualda et al., 2012) to calculate crystallization pressures based on the coexistence of quartz, sanidine, plagioclase, melt, and a fluid phase (following Bégué et al., 2014b; Gualda and Ghiorso, 2014; Pamukcu et al., 2015b). All calculations were performed using the same set of parameters: 1,000–700°C in 1°C intervals; 400–25 MPa in 25 MPa intervals; f_{O2} fixed at the Ni-NiO buffer; enough water added to ensure water saturation at all pressures investigated. The stability of Fe-free phases such as quartz and feldspars is not affected by f_{O2} conditions, so the specific choice of oxygen fugacity conditions is unimportant for our calculations. Further, Gualda and Ghiorso (2014) and Ghiorso and Gualda (2015) have demonstrated that the activity of H_2O does not appreciably affect the calculated pressures for quartz-2 feldspar assemblages—we thus used rhyolite-MELTS 1.0 for all calculations, assuming a pure-H_2O fluid phase (Ghiorso and Gualda, 2015). Crystallization pressures are calculated as the pressure at which the quartz, sanidine, and plagioclase saturation surfaces (as calculated by rhyolite-MELTS) intersect at the liquidus for the given melt composition (approximated by matrix glass analyses) used; if no intersection is found with a tolerance of 5 °C, no pressure is returned (for details, see Gualda and Ghiorso, 2014).

Zircon-saturation geothermometry

Crystallization temperatures were calculated using zircon-saturation geothermometry (Watson, 1979; Watson and Harrison, 1983; Hanchar and Watson, 2003; Boehnke et al., 2013), under the assumption that zircon equilibrated with melt preserved as glass in pumice clasts. Zircon is an ubiquitous phase in Bishop Tuff pumice (Hildreth, 1979; Reid and Coath, 2000; Simon and Reid, 2005; Hildreth and Wilson, 2007; Reid et al., 2011; Pamukcu et al., 2012; Chamberlain et al., 2014b), making the use of matrix glass compositions ideal for the application of zircon-saturation geothermometry. We present results using the calibration of Watson and Harrison (1983), which yields temperatures more consistent with other geothermometers for evolved rhyolitic compositions (Pamukcu et al., 2013; Foley et al., 2020). The relative differences in temperature among the various samples—the most critical aspect for our analysis—do not significantly change if the Boehnke et al. (2013) calibration is used.

Compositional group identification using multivariate analysis

In order to identify compositional groups within our compositional data, we performed multivariate statistical analysis. We compared matrix glass compositions by

calculating the Euclidean distance between the z-scores of the median values for each stratigraphic unit (distinguishing between the Vanderbilt and Chamberlain datasets). In order to eliminate the effect of wildly different absolute values for each oxide or element, the median of each oxide (for major elements measured by EDX-SEM) or element (for trace elements measured by LA-ICPMS) was normalized using the formula:

$$z_i = \frac{x_i - \bar{x}}{s}$$

where z_i is the z-score for oxide or element i, x_i is the median for that oxide or element, and $\bar{x}$ and s are, respectively, the average and standard deviation of the population of means for that oxide or element. The resulting z-scores are such that their average for each oxide or element is 0 and the corresponding standard deviation is 1. The Euclidean distance is then simply the square root of the sum of the squares of the differences between any two compositions (i.e., a Pythagorean distance in multidimensional space); we divide the value of the Euclidean distance by the square root of the number of oxides and elements used, so as to remove the effect of the number of components. We perform pairwise comparisons between all stratigraphic units.

Additionally, we performed a principal component analysis to identify the major axes of variability in the compositional data, so as to better contrast and compare the compositional data. In principal component analysis, a new set of orthogonal axes is calculated, with the first principal component representing the direction that captures the largest variability in the data, with each successive principal component representing the next orthogonal direction that shows most variability. In this sense, principal components help reduce the number of values that need to be considered to capture the variability observed in multidimensional space.

All multivariate calculations were performed in Microsoft Excel, taking advantage of functions distributed by *Real Statistics Using Excel* (http://www.real-statistics.com/).

Comparison of pressure and temperature populations using statistical analysis

In order to test if the different pressure and temperature populations have notably different means, we performed an Analysis of Variance (ANOVA), with pairwise comparisons using t-tests. We examined whether the samples were drawn from normally distributed populations using Shapiro-Wilk tests; and we compared the variances of the three groups to see if they are sufficiently similar. Because some of the assumptions needed for ANOVA may not be adequately satisfied by our data, we also performed the non-parametric Kruskal–Wallis test, with pairwise comparisons using Mann-Whitney tests. All calculations and tests were performed in Microsoft Excel with *Real Statistics Using Excel*.

Results

Geobarometry

Our results confirm the well-known fact that matrix glass in the Bishop Tuff is remarkably uniform in terms of silica content (see Figure 2, Figure 3, Figure 4), comprising almost exclusively high-silica rhyolite glass with 77.7 wt% SiO_2 (normalized anhydrous; Wallace et al., 1999; Anderson et al., 2000). Excluding four samples from unit Ig1Eb that have silica contents between 75.5 and 76.0 SiO_2 (see Hildreth and Wilson, 2007), all of the remaining samples from the Vanderbilt dataset have silica content between 76.5 and 78.5 wt%. Average and median SiO_2 values (both 77.7 wt% for early-erupted Bishop Tuff, 77.6 wt% for both East and North sectors late-erupted Bishop Tuff) are nearly identical with a very low standard deviation (0.3 and 0.2 wt%, respectively, 1-sigma). Results for the Chamberlain dataset are very similar (77.8 ± 0.4 wt% for early-erupted Bishop Tuff, 77.7 ± 0.5 wt% for East-sector late-erupted Bishop Tuff, 77.8 ± 0.4 wt% for North-sector late-erupted Bishop Tuff). This information alone suggests that the crystallization pressures for early and late-erupted Bishop Tuff should be very similar (Gualda and Ghiorso, 2013b).

Projection of matrix glass compositions from the Vanderbilt dataset onto the haplogranitic ternary (Figure 5) shows that crystallization pressures for Bishop Tuff pumice from all units studied are very similar, somewhere between the 100 and 200 MPa quartz-feldspar cotectic curves. While the inferred pressures are somewhat crude, their similarity is striking, suggesting no gradient in pressure between the three groups identified here. In fact, the only possible deviation is that North-sector late-erupted matrix-glass compositions suggest slightly lower crystallization pressures than early-erupted and East-sector late-erupted matrix-glass compositions.

Application of the rhyolite-MELTS geobarometer confirms the inference made based on SiO_2 content of matrix glass, as well as on the projection of matrix-glass compositions onto the haplogranitic ternary. Average crystallization pressures—for an assemblage including quartz and two feldspars in equilibrium with melt of the measured composition—are nearly identical for both early-erupted (140 MPa, n = 95) and East-sector late-erupted (136 MPa, n = 49) pumice; North-sector late-erupted pumice shows slightly lower crystallization pressures (118 MPa, n = 18). Median values show the same results (133, 135, and 115 MPa, respectively). The observed standard deviations (24, 17, and 15 MPa, respectively, 1-sigma) are comparable with the uncertainty of the rhyolite-MELTS geobarometer (~25 MPa, 1-sigma; see Gualda and Ghiorso, 2014), suggesting that all values observed belong to single populations of pressures. Overall, the rhyolite-MELTS pressures confirm the inference made above that pressures for the three groups are very similar—the only possible deviation is that North-sector late-erupted pressures could be lower than those for the other two groups.

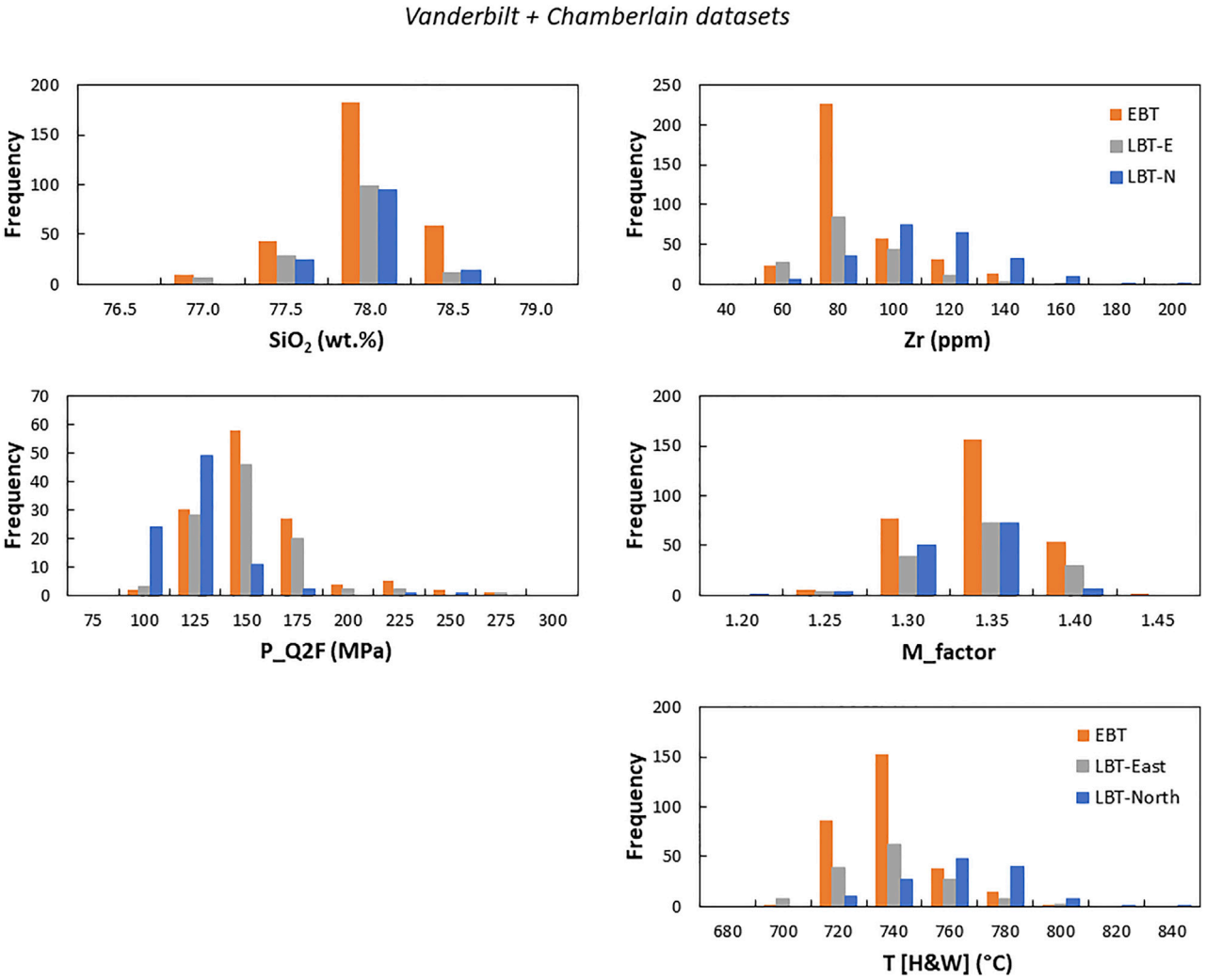

FIGURE 2
Histograms showing the distribution of select compositional parameters (SiO_2, Zr, M-factor) for Bishop Tuff matrix glass, as well as rhyolite-MELTS pressures and zircon-saturation temperatures calculated from these data. Data from this study and from Chamberlain et al. (2015) included in all diagrams. Data are divided into early-erupted (EBT), East-sector late-erupted (LBT-E) and North-sector late-erupted (LBT-N), as illustrated in Figure 1. P_Q2F is calculated using the rhyolite-MELTS geobarometer (Gualda and Ghiorso, 2014) using a mineral assemblage composed of quartz and two feldspars (see text for details). Zircon saturation temperatures (T) are calculated using the calibration of Watson and Harrison (1983). Note that SiO_2 and P_Q2F are all very similar for all units. Zr and T are very similar for early-erupted and East-sector late-erupted pumice, while North-sector late-erupted pumice yields modes that are Zr ~ 20 ppm and T ~ 20–30°C higher.

Results of our ANOVA comparing the three populations of quartz-2 feldspar rhyolite-MELTS pressures suggest that the three populations do not have the same means (p-value of ~$5x10^{-4}$), but the pairwise comparisons suggest that pressure populations for early-erupted and East-sector late-erupted matrix glass have statistically indistinguishable means (p-value of 0.24). In contrast, the pressure population for North-sector late-erupted matrix glass differs significantly from both early-erupted (p-value of $1x10^{-5}$) and East-sector late-erupted (p-value of $2x10^{-4}$) matrix-glass pressures. However, there are substantial differences in the number of pressures for each group (75 pressures for early-erupted pumice; 49 for East-sector late-erupted pumice; and 18 for North-sector late-erupted pumice), and the Shapiro-Wilk test results suggest that the distribution of pressures for early-erupted pumice is not normal (p-value of $4x10^{-4}$)—pressure populations for both East-sector and North-sector late-erupted pumice can be considered normal (p-values of 0.37 and 0.16, respectively). These results suggest it may be preferable to perform a non-parametric test instead of ANOVA. The results of the Kruskal–Wallis test are very similar to the ANOVA, suggesting that the three populations are not all equal (p-value of $1x10^{-4}$). Pairwise comparisons using

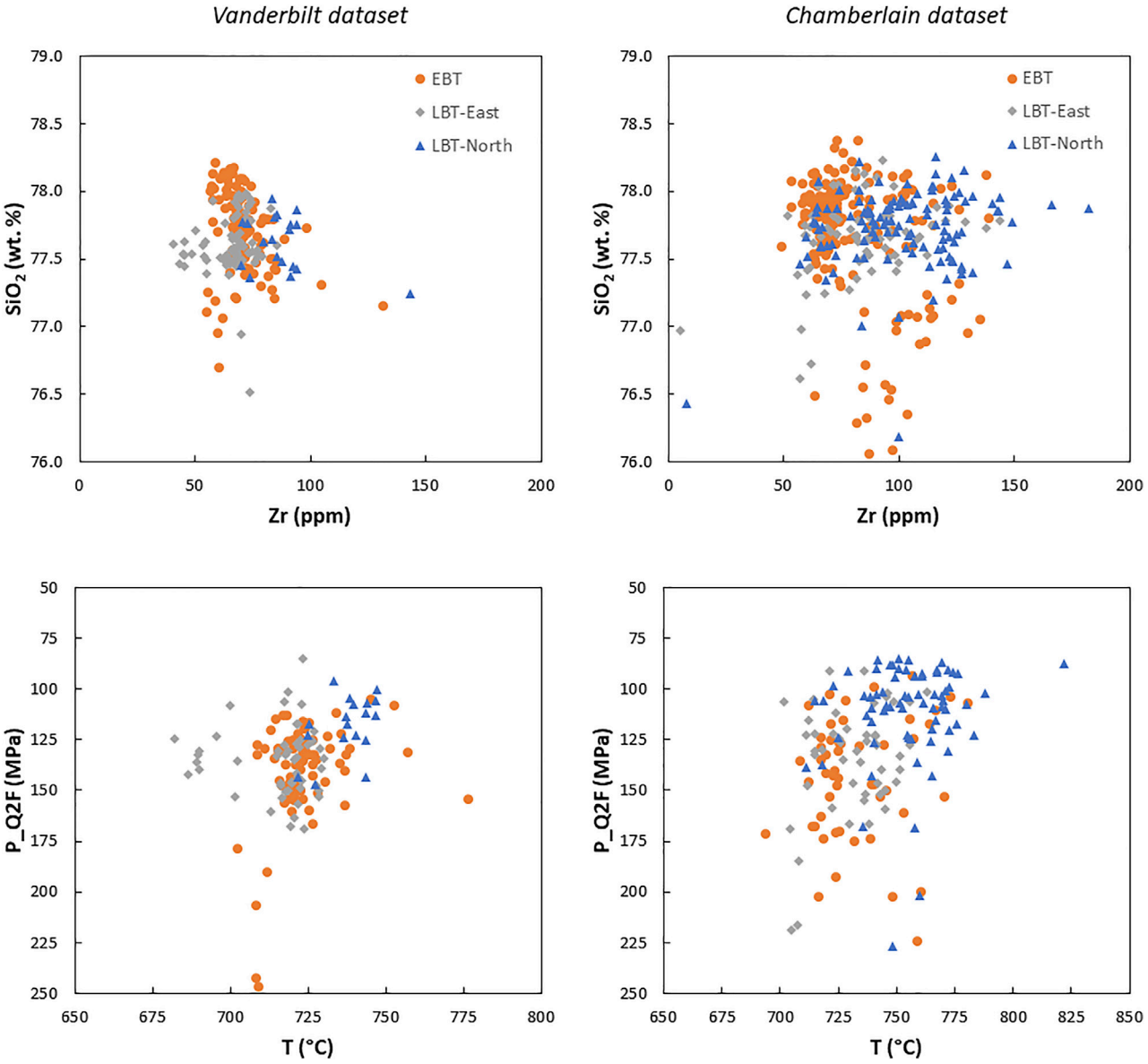

FIGURE 3
Scatter diagrams showing compositions (SiO_2 and Zr in glass) and intensive parameters (temperature and pressure) for pumice from the Bishop Tuff for the Vanderbilt (this study) and Chamberlain (Chamberlain et al., 2015) datasets. Data are divided into early-erupted (EBT), East-sector late-erupted (LBT-East) and North-sector late-erupted (LBT-North), as illustrated in Figure 1. Note the large overlap between the various parts of the deposit, particularly for the Vanderbilt dataset. Zr contents and zircon-saturation temperatures extend to higher values for the Chamberlain dataset. Importantly, there are no distinguishable trends in pressure versus temperature space, as would be expected by the model of Hildreth (1979).

Mann-Whitney tests also suggest that early-erupted and East-sector late-erupted pressure populations do not have notably different distributions (p-value of 0.90), while they both have significantly different distributions than North-sector late-erupted pressures (p-values of $2x10^{-5}$ and $2x10^{-4}$, respectively). The statistical tests emphasize that the distributions of pressures for early-erupted and East-sector late-erupted pumice are very similar, but that the distribution for North-sector late-erupted is significantly different from the others. Since the histograms reveal similarly shaped distributions, the results from these non-parametric tests imply that the North-sector late-erupted pressure population has mean and median pressures that are statistically lower than the early-erupted and East-sector late-erupted mean and median pressures. In this sense, the ANOVA and Kruskal–Wallis tests reject the hypothesis of vertical stratification of the Bishop Tuff magma

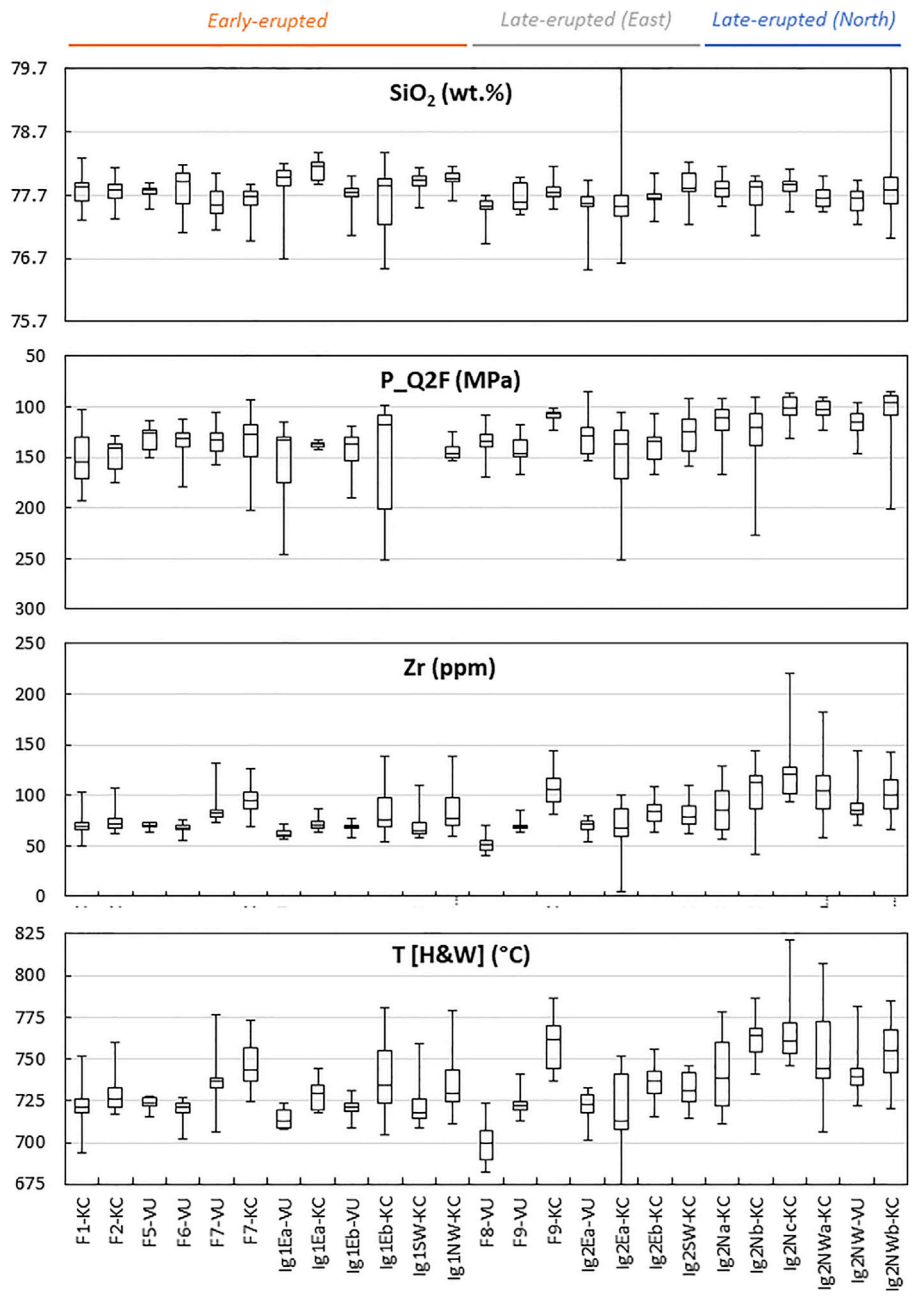

FIGURE 4A
Box and whisker diagrams showing the distribution of compositional parameters (SiO_2, Zr, Nb, Ce, Rb, Th) and intensive parameters (pressure and temperature) for glass from the Bishop Tuff. Diagrams are divided into each depositional unit (following Wilson and Hildreth, 1997), per dataset (i.e., VU for Vanderbilt dataset, and KC for Chamberlain dataset). Units are placed in approximate stratigraphic order (the relative stratigraphic positions of East-sector and North-sector late-erupted Bishop Tuff are unknown).

body, which would imply increasing means and medians from early-erupted to East-sector late-erupted to North-sector late-erupted pumice.

Results from the Chamberlain dataset are very similar to ours, with slightly higher average and median pressures for early-erupted Bishop Tuff, and somewhat larger standard deviations (early-erupted Bishop Tuff: 146 ± 33 MPa, median 142 MPa; East-sector late-erupted Bishop Tuff: 137 ± 32 MPa, median 130 MPa; North-sector late-erupted Bishop Tuff: 111 ± 25 MPa, median 106 MPa). Despite the small differences, the results show very similar pressures for both early-erupted and East-sector late-erupted Bishop Tuff, with North-sector late-

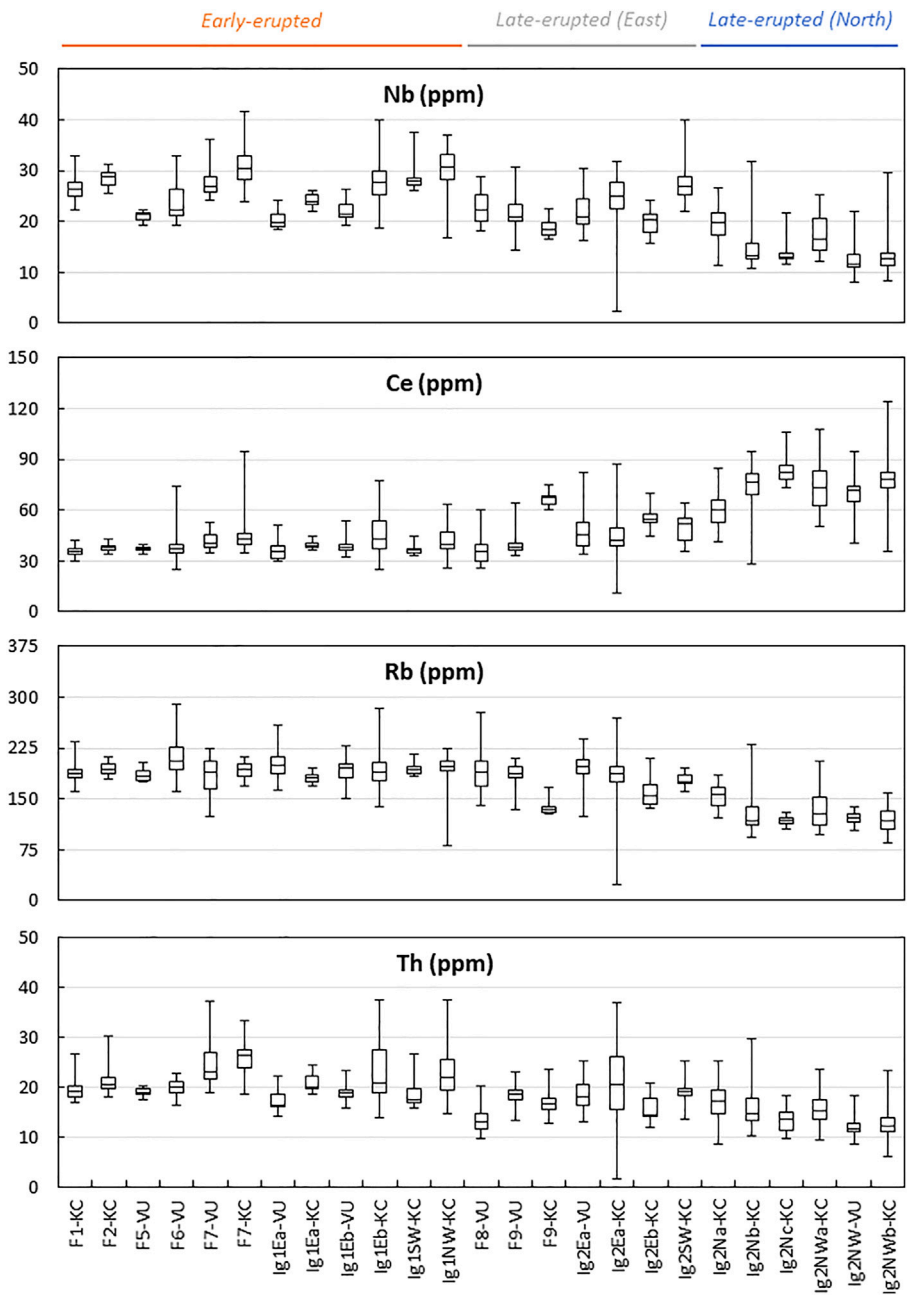

FIGURE 4B

erupted Bishop Tuff again showing somewhat lower crystallization pressures.

Geothermometry

Matrix glass Zr content varies over a relatively narrow range for all samples (see Figure 2, Figure 3, Figure 4). In the Vanderbilt dataset, early-erupted and East-sector late-erupted pumice clasts have very similar distributions (71 ± 10, 66 ± 10 ppm, medians of 69 and 68 ppm, respectively), while North-sector late-erupted pumice clasts show somewhat higher Zr values (88 ± 16 ppm, median 86 ppm). Given the fact that major-element compositions are also fairly similar, the compositional factor M (used for zircon saturation temperature calculations) shows very tight distributions for all groups in both datasets (average

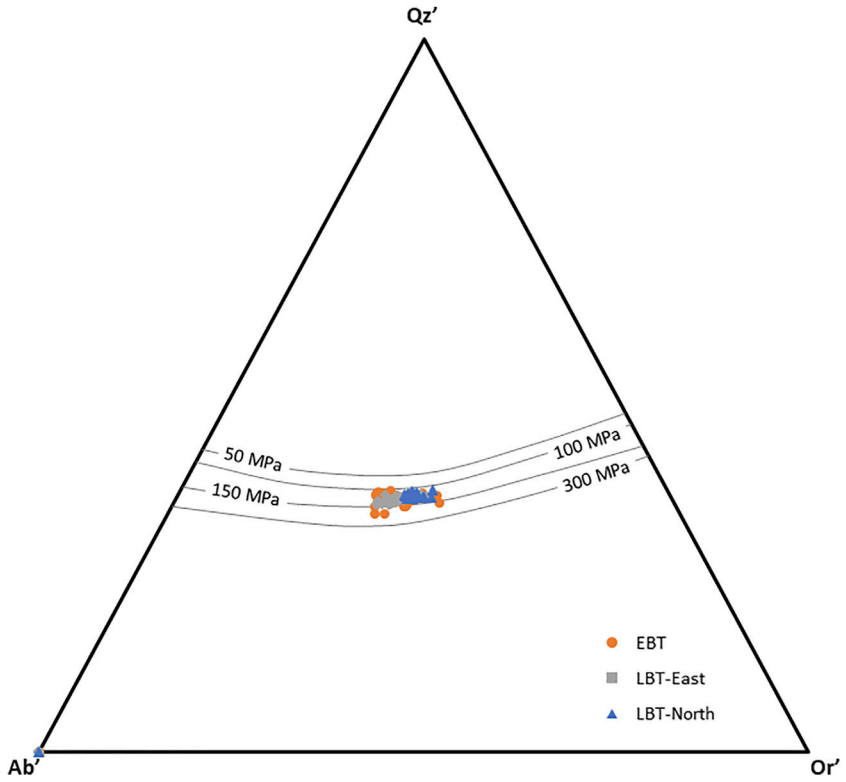

FIGURE 5
Projection of matrix-glass compositions of the Bishop Tuff onto the haplogranitic ternary. Compositions are projected using the scheme of Blundy and Cashman (2001), which was developed for metaluminous compositions. Compositions which yield normative corundum larger than 0.5 are not plotted. Note that the vast majority of compositions fall between the 100 and 200 MPa cotectic curves, and that there is no systematic difference in inferred pressure between early-erupted, East-sector late-erupted, and North-sector late-erupted magmas.

and median of 1.32–1.33 for the Vanderbilt dataset, and 1.30–1.31 for the Chamberlain dataset, all with standard deviation smaller than 0.04). It thus results that crystallization temperatures derived from zircon-saturation geothermometry are similarly distributed for early and East-sector late-erupted pumice, and they are somewhat higher for North-sector late-erupted pumice (Figure 2; average temperatures of 723, 718, and 740°C; median 722, 721, and 739°C; standard deviation of 11, 12, and 13°C, n = 113, 71, 19, respectively). In essence, there is no significant difference in temperature between early-erupted and East-sector late-erupted crystallization temperatures, with slightly higher (~20°C) temperatures for North-sector late-erupted Bishop Tuff pumice.

None of the temperature populations follow normal distributions according to the Shapiro-Wilk test. Accordingly, only non-parametric tests were employed. Results of the Kruskal–Wallis test suggest a very low probability that all three populations are equivalent (p-value of $1x10^{-8}$). Pairwise Mann-Whitney tests suggest that the distribution of temperatures for early-erupted and East-sector late-erupted pumice are more similar to each other (p-value of 0.04) than North-sector late-erupted temperature populations (p-value of 1×10^{-7} when comparing early-erupted and North-sector late-erupted temperature populations; and p-value of 1×10^{-8} when comparing East-sector and North-sector late-erupted temperature populations). In summary, our results support similar temperatures for early-erupted and East-sector late-erupted magmas, and temperatures that are significantly different for North-sector late-erupted magmas—comparison of the mean and median values for each population suggest that temperatures for North-sector late-erupted magmas could be ~20°C higher (but not greater) than the temperatures experienced by the other two groups.

Results obtained using the Chamberlain dataset are again very similar to ours (early-erupted Bishop Tuff: 733 ± 17°C, median 727°C; East-sector late-erupted Bishop Tuff: 734 ± 29°C, median 738°C; North-sector late-erupted Bishop Tuff: 754 ± 21°C, median 755°C), again suggesting a maximum temperature difference of ~20°C higher for North-sector late-erupted magmas when compared to early-erupted and East-sector late-erupted magmas.

Importantly, the ubiquitous presence of zircon in Bishop Tuff pumice (Reid and Coath, 2000; Simon and Reid, 2005; Reid et al.,

2011; Chamberlain et al., 2014b) and the systematically higher Zr concentrations for whole-rock when compared to glass compositions (Hildreth, 1979; Hildreth and Wilson, 2007) support the idea that Bishop Tuff magmas were zircon-saturated, and zircon-saturation temperatures actually record pre-eruptive conditions.

Combined crystallization pressures and temperatures

In the Vanderbilt dataset, a total of 149 compositions yielded both a rhyolite-MELTS pressure and a zircon saturation temperature. Comparison of Zr and SiO_2 values and of zircon-saturation temperatures and quartz-2 feldspars rhyolite-MELTS pressures (Figure 3) shows complete overlap between results for early-erupted and East-sector late-erupted pumice, with North-sector late-erupted results displaced to slightly higher values of Zr and T, and lower values of P. In the Chamberlain dataset, a total of 181 compositions yielded both temperatures and pressures of crystallization; similarly, there is complete overlap between early-erupted and East-sector late-erupted pumice, with higher Zr and T and slightly lower P for North-sector late-erupted pumice (Figure 3), even if the range of temperatures is a bit wider in the Chamberlain dataset when compared to the Vanderbilt dataset.

Matrix glass compositions

Differences in matrix glass compositions are mostly subtle, particularly for major elements. Yet, there are systematic variations in both datasets (Figure 4). As a general trend, Ce and Ba values increase from early-erupted to East-sector late-erupted to North-sector late-erupted glass, while Nb, Y, Rb, and Li decrease in that direction. North-sector late-erupted units show the most pronounced differences from the remainder of the dataset. Fall unit F8 compositions tend to be—at least for some elements—more similar to early-erupted units than late-erupted units, which is interesting given that this unit formed during an important transition in the Bishop supereruption (Wilson and Hildreth, 1997). Flow unit Ig1Eb shows significant compositional variability, with noticeable differences in the compositional spectrum observed in each outcrop of the unit—this is consistent with the fact that Ig1Eb does not correspond to a single flow, but rather to a series of flows that appear at approximately the same stratigraphic level (Wilson and Hildreth, 1997). Finally, values for unit Ig2Na seem to be closer to values from late-erupted East-sector units than to late-erupted units from the North sector, suggesting that magmas akin to East-sector magmas also deposited to the North.

Results of our principal component analysis (Figure 6) show that almost 60% of the variability observed in our dataset is captured by principal component 1 (PC1), while PC2 explains 15% of the variability. The first five principal components explain more than 90% of the total variability. This shows that the variability can be explained very well by the first few principal components. Our results (Figure 6) show that PC1 varies strongly as a function of stratigraphic position: early-erupted matrix glass has the lowest values of PC1 (all negative), while North-sector late-erupted glass shows the highest values (all positive), with East-sector glass displaying values of PC1 in between (close to zero). The values for PC1 also suggest that matrix glass from Ig2Na is compositionally more similar to those from East-sector late-erupted compositions, even though it deposited in the North sector. We do not see any systematic variation in higher order principal components (see results for PC2 in Figure 6) as a function of stratigraphic position.

Inspection of the compositional results (Figure 7) reveals the existence of three groups of elements (or oxides): 1) elements enriched in North-sector late-erupted matrix glass; 2) elements enriched in early-erupted matrix glass; 3) elements whose variability is not systematic when comparing early-erupted and North-sector late-erupted compositions. This subdivision was initially performed by inspection, but later confirmed by the fact that group 1 corresponds to elements with loading factor >0.65 for principal component 1, while group 2 includes elements with loading factor <−0.65, with elements in group 3 displaying loading factor between −0.54 and 0.46. This means that elements in groups 1 and 2 explain most of the variability observed in PC1. In Figure 7, the cell background is colored on a color scale from orange to blue, such that, for group 1 elements, the lowest value in each row of elements is colored orange, while the highest value is colored blue, with values in between colored in lighter shades, with the average value corresponding to white. For group 2 elements, the lowest value is colored blue and the highest value orange (i.e., reverse color scheme as group 1), so as to emphasize the same compositional groups as in group 1. The variations in major and trace-element compositions—as illustrated by the color coding in Figures 7 – confirm the results from the principal component analysis, illustrating the compositional differences between early-erupted, East-sector late-erupted, and North-sector late-erupted magmas.

Elements in group 3 were colored from green (low values) to red (high values), and show much more scattered results than elements in groups 1 and 2. Interestingly, as mentioned above, SiO_2—which correlates strongly with crystallization pressure for high-silica rhyolites (Gualda and Ghiorso, 2013b)—is among the elements that shows no systematic correlation with stratigraphy; in fact, SiO_2 has a loading factor of only -0.17, showing that it does not contribute significantly to PC1, which is the only principal component to vary with stratigraphy. This reinforces the result that pressure does not vary with stratigraphy in the Bishop Tuff.

The matrix of Euclidean distances (Figure 8) displays values for the Euclidean distance for each pair indicated in

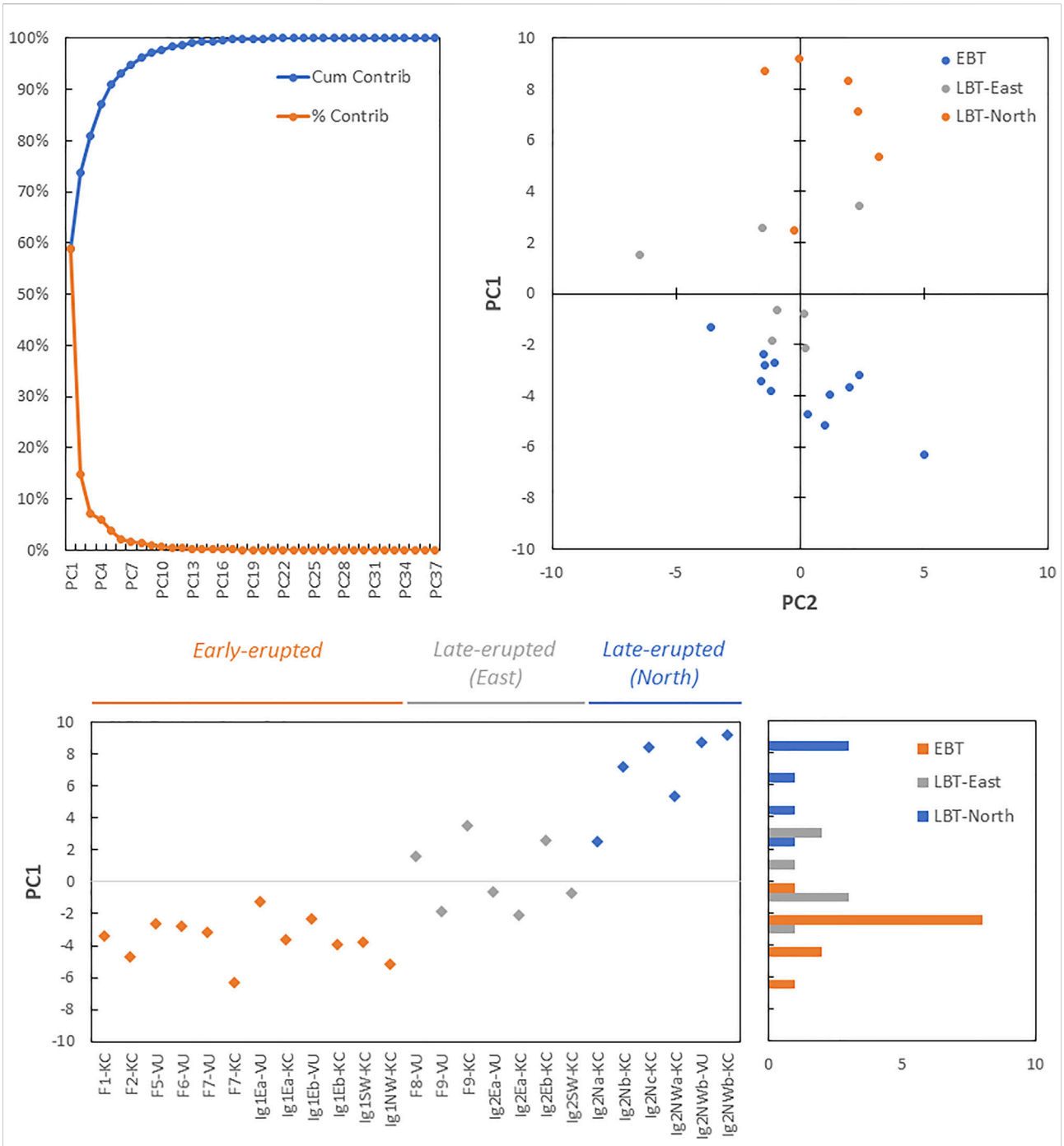

FIGURE 6
Results of principal component analysis using matrix glass compositions from Bishop Tuff pumice. Top left diagram shows the relative and cumulative contributions of each principal component to the total variability observed in the compositional data. Top right diagram shows the variation of PC1 vs. PC2 for each portion of the deposit (early-erupted in blue; East-sector late-erupted in gray; and North-sector late-erupted in orange). Bottom left diagram shows variation in PC1 as a function of stratigraphy, while the bottom right bar diagram shows the distribution of PC1 values for each portion of the deposit. Principal component 1 (PC1) captures most of the variability observed in the data, and varies systematically with stratigraphy, suggesting the presence of three compositional groups. In contrast, higher order principal components represent ≤15% of the variability (see top left diagram), and they do not vary systematically with stratigraphy (as seen by PC2 in top right diagram).

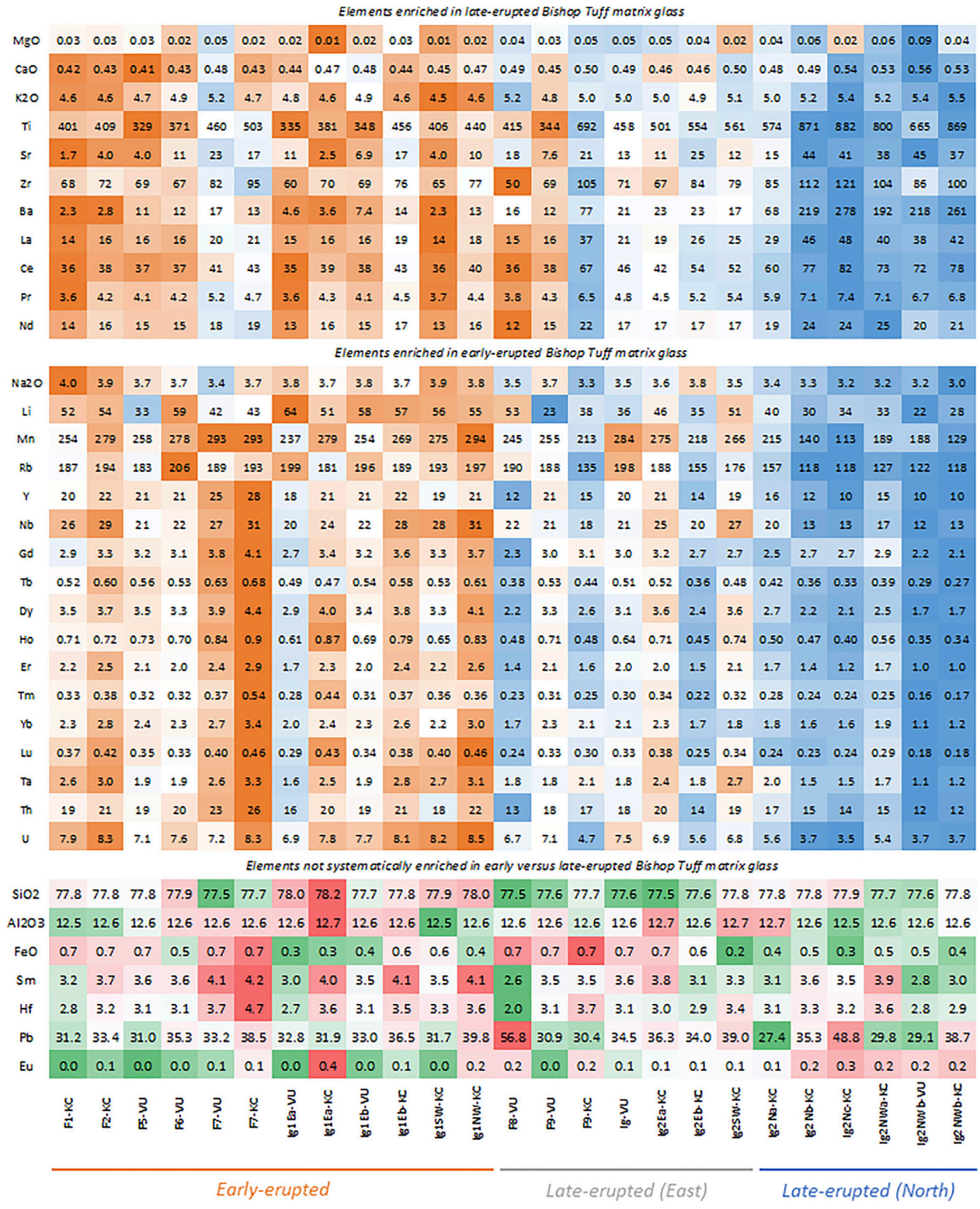

FIGURE 7
Compositions of matrix glass from the Bishop Tuff. Elements are organized in three groups, as indicated. Background color correlates linearly with concentration, with the color scheme being reversed between the top two groups, to emphasize the same compositional groups. Elements in the third group are colored using different colors, to emphasize the lack of systematic variation with stratigraphy. While separation of oxides and elements into the three groups was initially done by inspection, it was later confirmed by the principal component analysis, which reveals significantly different loading factors for each of the three groups (loading factors for group 1 are >0.65 for principal component 1; < −0.65 for group 2; and between −0.54 and 0.46 for group 3). The presence of the three groups is confirmed by the concentrations shown here (particularly by the color coding). See text for details.

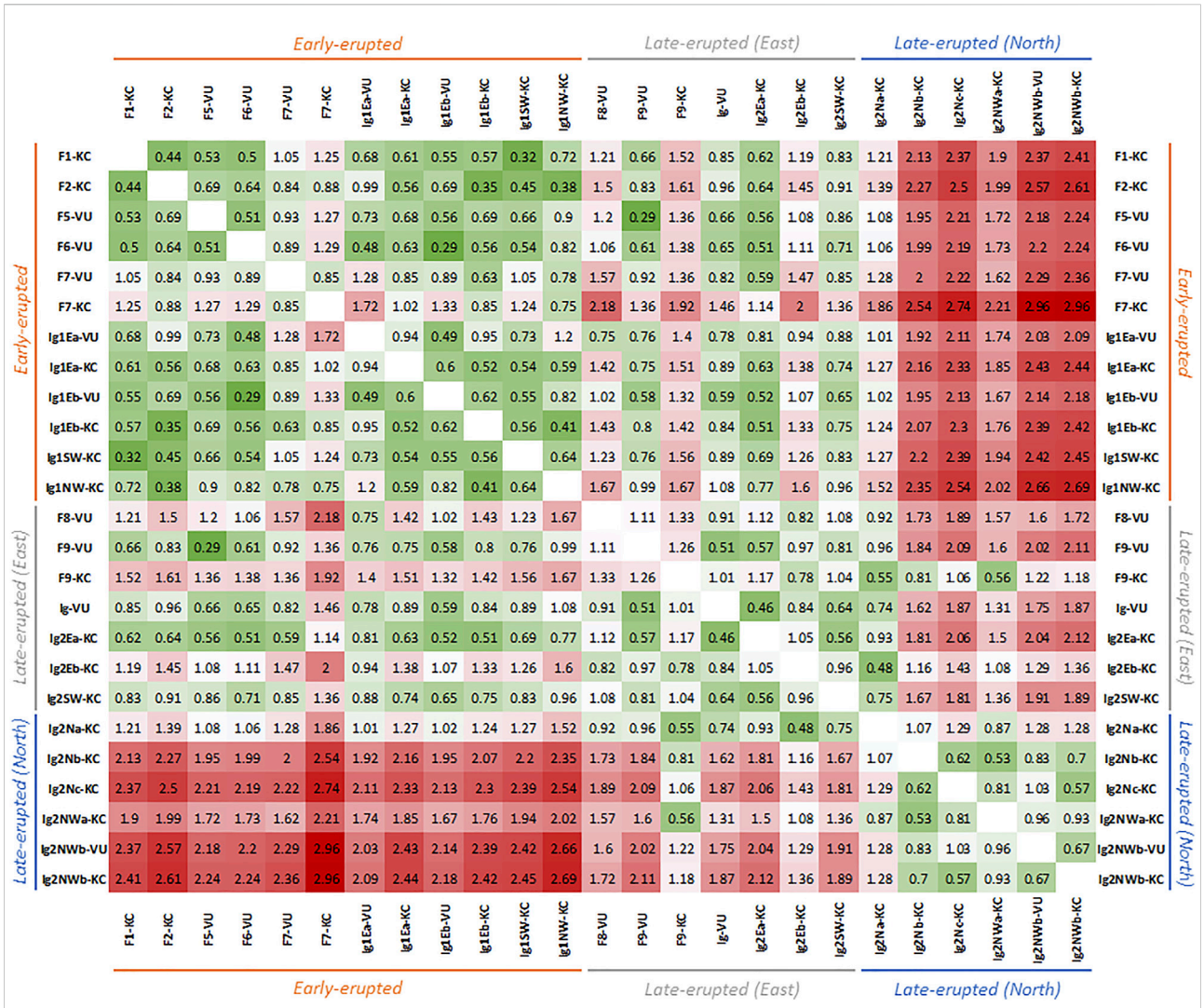

FIGURE 8
Matrix of Euclidean distances between pairs of stratigraphic groups. Low values appear in shades of green, while high values appear in shades of red. Note that the matrix is symmetric. The three stratigraphic groups are revealed by the small distances (green shading) within each group, but with larger differences from other groups. The contrast between early-erupted and North-sector, late-erupted compositions is most evident, with East-sector, late-erupted compositions showing more variable distances to these two endmember groups.

the table. Only elements in groups 1 and 2 were included in the calculation of the Euclidean distance. Green shading corresponds to low values (i.e., small distances), while red shading is used for high values (note that the matrix is symmetric about its diagonal). The results make it clear that North-sector late-erupted glass compositions form a coherent group (small distances within the group, large distances to units from other groups), and similarly for early-erupted glass. East-sector late-erupted glass also forms a coherent group, with results suggesting somewhat higher variability within the group—consistent with results from the principal component analysis and from inspection of the compositions.

In summary, our analysis shows strong evidence for the existence of three groups of glass compositions in the Bishop Tuff deposits, which are systematically distributed stratigraphically. The distribution of values for PC1 indicates three discrete groups, rather than a continuous gradient in compositions—the same can be grasped from careful study of the matrix of Euclidean distances (Figure 8).

Discussion

Our results reveal a very clear pattern of crystallization pressures, temperatures, and compositions for magmas from

the Bishop Tuff, with important implications for the architecture of the magmatic system that fed the Bishop Tuff supereruption.

Crystallization pressures

As emphasized by Gualda and Ghiorso (2013a) the original idea of a single, vertically stratified magma body derives almost exclusively from the general stratigraphy of the deposit itself, which suggests eruption of magmas that formed the early-erupted Bishop Tuff prior to eruption of the magmas that formed the late-erupted deposits. Neither Hildreth (1979) nor Hildreth and Wilson (2007) provide any direct estimates of pre-eruptive crystallization pressure. Importantly, Wilson and Hildreth (1997) emphasize the complexity of the eruption sequence, and the pitfalls in using it as a guide to the structure of the magma body underneath. Direct evidence for crystallization pressures comes primarily from the works of Wallace et al. (1999) and Anderson et al. (2000), who used H_2O-CO_2 concentrations in glass inclusions to calculate crystallization pressures; and from Gualda and Ghiorso (2013a), who calculated melt inclusion entrapment pressures using the rhyolite-MELTS geobarometer (Gualda and Ghiorso, 2014). We complement these data with crystallization pressures calculated from matrix glass compositions using the rhyolite-MELTS geobarometer.

Overall, our results show very similar crystallization pressures for all units and compositional groups. Crystallization pressures for North-sector late-erupted magmas are slightly lower (~20 MPa, ~0.75 km) than those for early-erupted and East-sector late-erupted magmas. These results are similar to what Gualda and Ghiorso (2013a) documented using quartz-hosted glass inclusion compositions (using the compositions from Wallace et al., 1999; Anderson et al., 2000), which show very similar pressures for early and late-erupted Bishop Tuff. While Wallace et al. (1999) and Anderson et al. (2000) interpret H_2O-CO_2 compositions of glass inclusions as being consistent with the vertical stratification proposed by Hildreth (1979) and later advocated by Hildreth and Wilson (2007), the H_2O-CO_2 pressures primarily show overlap in their distribution for early-erupted and late-erupted magmas (see Figure 9 in Wallace et al. (1999). The interpretation of Wallace et al. (1999) and Anderson et al. (2000) hinges on the assumption that late-erupted magmas were fluid-undersaturated, such that H_2O-CO_2 pressures represent minimum pressures. The combination of the results of Wallace et al. (1999) and Anderson et al. (2000) with the pressures calculated by Gualda and Ghiorso (2013a) suggests that most or all Bishop Tuff magmas were fluid-saturated at the time of melt inclusion entrapment—in other words, the agreement between the pressures calculated by Gualda and Ghiorso (2013a) and H_2O-CO_2 pressures suggests that melt inclusions were entrapped under fluid-saturated conditions (i.e., otherwise H_2O-CO_2 pressures would be systematically higher than rhyolite-MELTS pressures). Our results here further reinforce this idea, showing similar pressures for all magmas at the time of eruption.

Treated in combination, the results of Wallace et al. (1999), Anderson et al. (2000), Gualda and Ghiorso (2013a), and from this study all suggest crystallization over a small range of pressures that do not lend support to the inferences originally made by Hildreth (1979) based on the general stratigraphy of the deposit. In this context, there is overwhelming evidence that all estimates of crystallization pressure derived to date show variation over a similar range for all units of the Bishop Tuff (with North-sector late-erupted magmas crystallizing at slightly lower pressures than the other groups), consistent with lateral juxtaposition of magmas that fed the Bishop Tuff eruption, in agreement with the conclusions of Gualda and Ghiorso (2013a).

In fact, comparison of the distribution of pressures for each of the subgroups identified here (i.e., early-erupted, East-sector late-erupted, and North-sector late-erupted) rules out vertical stratification of the three different groups, and further suggests that each group erupted from a magma body which spanned a similar depth range. The maximum depth range occupied by each magma body is given by the range of pressures seen in Figure 2 and Figure 3 (~75 MPa; or 2.8 km, assuming an average density of $2.7x10^3$ kg/m^3 for the overlying crust). However, the thickness of each body is likely much better approximated by the uncertainties associated with the mean value for each population (i.e., the standard deviation), which suggest pressure ranges of 30–50 MPa (2-sigma), or thicknesses of 1.1–1.9 km, consistent with inferences based on glass inclusions by Anderson et al. (2000).

Crystallization temperatures

The results of Fe-Ti oxide geothermometry originally obtained by Hildreth (1979) have greatly influenced our thinking about the Bishop Tuff, in particular, and about giant magma bodies that feed supereruptions more generally. Combined with inferences based on the stratigraphy of the deposit, Fe-Ti oxide temperatures were interpreted by Hildreth (1979) to record a thermal gradient of over 100°C as a function of depth within the pre-eruptive Bishop Tuff magma body. These variations in Fe-Ti oxide temperatures were later reproduced using more extensive datasets and by other authors (Hildreth and Wilson, 2007; Jolles and Lange, 2019), which have lent some confidence to the findings. While these more recent measurements confirm the validity of the compositional results obtained by Hildreth (1979), the significance of the calculated temperatures is still debatable. Oxygen isotope compositions of quartz and magnetite have been interpreted to represent thermal gradients of ~100°C between early-erupted and late-erupted Bishop Tuff magmas (Bindeman and Valley, 2002). However,

Gualda et al. (2012) and Ghiorso and Gualda (2015) demonstrate that such a large temperature gradient is inconsistent with phase-equilibria considerations; Ghiorso and Gualda (2013) further argue that Fe-Ti oxides were not in equilibrium with melt compositions preserved in Bishop Tuff pumice; and, finally, Gualda and Ghiorso (2013a) show that zircon-saturation temperatures are also inconsistent with the large thermal gradient inferred from the Fe-Ti oxides. Evans and Bachmann (2013) and Evans et al. (2016) suggest that Fe-Mg minerals are potentially in equilibrium with Fe-Ti oxides, and they question the significance of zircon-saturation temperatures based on glass inclusions discussed by Gualda and Ghiorso (2013a). These results reveal a complex temperature record for the Bishop Tuff, and they beg the question as to which proxy (or proxies) record pre-eruptive conditions, and what might be the significance of other proxies. We review these topics in greater detail below.

While many applications of zircon-saturation geothermometry have focused on whole-rock data, particularly for granites (e.g., Hanchar and Watson, 2003; Miller et al., 2003), zircon-saturation geothermometry is ideally suited when using glass compositions for magmas that can be demonstrated to be saturated in zircon. The ubiquity of zircon in Bishop Tuff pumice (Hildreth, 1979; Bindeman and Valley, 2002; Simon and Reid, 2005; Hildreth and Wilson, 2007; Reid et al., 2011; Chamberlain et al., 2014b) leaves little doubt that Bishop Tuff magmas were zircon-saturated; further, the presence of large proportions of zircon that yield ages within error of the eruption (Simon and Reid, 2005) suggest that Bishop Tuff magmas were zircon-saturated under pre-eruptive conditions. Gualda and Ghiorso (2013a) present zircon-saturation temperatures using glass inclusion data from the literature (Wallace et al., 1999; Anderson et al., 2000); the results support only small (<30°C) temperature differences between late-erupted and early-erupted magmas. One of the concerns raised by Chamberlain et al. (2015) is that glass inclusions used by Gualda and Ghiorso (2013a) are not representative of conditions immediately prior to eruption. Here we use a much more extensive set of samples, which spans a wider range of stratigraphic units from the Bishop Tuff. Nonetheless, we find no reliable evidence of pre-eruptive crystallization temperatures greater than ~750°C, suggesting that any variations in temperature observed in the Bishop Tuff magmas should not have been greater than 20–30°C—again in agreement with Gualda and Ghiorso (2013a). Evans et al. (2016) argue that the similarity of temperatures between early-erupted and late-erupted glass inclusions reported by Gualda and Ghiorso (2013a) stems from the fact that glass inclusions do not record the last equilibration of late-erupted magmas after rejuvenation by more primitive, hotter magma. Our results effectively rule out this hypothesis, given that East-sector late-erupted matrix glass yields temperatures (723 ± 11°C) indistinguishable from early-erupted matrix glass (718 ± 12°C), and North-sector late-erupted matrix glass results in temperatures (740 ± 13°C) that are < 25°C hotter than the other groups.

Our temperature estimates based on zircon-saturation geothermometry are in excellent agreement with the results of Ghiorso and Gualda (2015), which demonstrate that temperature variations due to the effect of reduced water activity in the melt (resulting from the presence of a mixed H_2O-CO_2 fluid) are on the order of 20°C for the range of CO_2 values observed for Bishop Tuff glass inclusions. In light of the small pressure variations we observe (see above), the similarity in pre-eruptive temperatures is not surprising and these temperature estimates are consistent with the experimentally determined phase diagram for late-erupted Bishop Tuff magma (Gardner et al., 2014). While the experiments of Klimm et al. (2008) suggest that large variations of temperature are possible, variations in the concentration of H_2O of more than 3 wt% would be needed to achieve a 100°C temperature gradient, which is inconsistent with the current evidence for H_2O-CO_2 values in Bishop Tuff magmas. Interestingly, the slightly higher crystallization temperatures we infer for North-sector late-erupted magmas are consistent with the lower pressures we estimate for these magmas for crystallization under fluid-saturated conditions.

Finally, Bindeman and Valley (2002) present data on oxygen isotope compositions of quartz and magnetite from the Bishop Tuff. They find differences in the average compositions between the early-erupted and late-erupted pumice clasts from their study, which can be interpreted to represent a temperature difference of ~100°C between early-erupted and late-erupted magmas. However, Bindeman and Valley (2002) also document significant variability in the oxygen isotope values within each group, beyond what can be explained by analytical uncertainty, with significant overlap between the populations for early-erupted and late-erupted samples. Critically, Bindeman and Valley (2002) also find significant variations in oxygen-isotope compositions between different zones of quartz crystals, particularly for the late-erupted samples. This is significant given that Bishop Tuff quartz—particularly in late-erupted samples—shows complex zoning, with common bright-CL rims (Peppard et al., 2001; Wark et al., 2007; Gualda and Sutton, 2016) that have been variously interpreted to represent different conditions of crystallization close to or during syn-eruptive ascent. Nonetheless, much of the difference in inferred temperature between the early-erupted and late-erupted samples of Bindeman and Valley (2002) derives from the oxygen-isotope compositions of magnetite. Given the evidence for the lack of equilibration between Fe-Ti oxides presented here, as well as the intra-crystal variations in oxygen-isotope composition in quartz, it is not clear whether the oxygen-isotope temperatures calculated by Bindeman and Valley (2002) reliably represent pre-eruptive conditions for Bishop Tuff magmas. Further work is necessary to reconcile the oxygen-isotope results with the phase-equilibria considerations presented here.

It is apparent from available results on glass inclusions (Gualda and Ghiorso, 2013a) and matrix glass (this study) that the large temperature variations inferred from Fe-Ti oxides and oxygen-isotope compositions of quartz and magnetite crystals are not representative of pre-eruptive conditions. It is well known that Fe-Ti oxides re-equilibrate rapidly under magmatic conditions (Van Orman and Crispin, 2010; Tomiya et al., 2013), on timescales of days to weeks. In this sense, the disagreement between temperatures recorded by glass equilibration with zircon and the equilibration between touching magnetite-ilmenite pairs is not totally unexpected (see Pitcher et al., 2021), particularly considering the evidence for substantial syn-eruptive crystallization in the Bishop Tuff (Pamukcu et al., 2012, 2016; Gualda and Sutton, 2016). Direct evidence that melt did not equilibrate with the current Fe-Ti oxide compositions was found by Ghiorso and Gualda (2013), who demonstrate that the activity of titania inferred from Fe-Ti oxides does not fall within a reasonable range expected for Bishop Tuff magmas—this means that the Fe-Ti oxides did not equilibrate with the melt with which they were in contact. We note that the Fe-Ti geothermo-oxybarometer of Ghiorso and Evans (2008) is built to be internally consistent with rhyolite-MELTS (Gualda et al., 2012), such that the disagreement cannot be explained by inconsistencies in the calibrations used. Further evidence for disequilibrium between Fe-Ti oxides in late-erupted Bishop Tuff pumice and the rhyolitic melt in which they reside is presented by Gardner et al. (2014). If Evans and Bachmann (2013) are correct that Fe-Mg minerals are in equilibrium with Fe-Ti oxides, then it would follow that Fe-Mg minerals are also not in equilibrium with the melt. We conclude that pre-eruptive conditions are recorded with much greater fidelity by equilibration of melt with quartz, feldspars, and zircon—in combination, these results suggest crystallization temperatures of ~720°C for early-erupted and East-sector late-erupted magmas, and slightly higher temperatures (~740 °C) for North-sector late-erupted magmas.

Magma compositions and their distribution

In his original work, Hildreth (1979) presents a number of diagrams showing correlations between Fe-Ti oxide temperatures and mineral compositions. From such diagrams, Hildreth (1979) infers a compositional gradient well correlated with the Fe-Ti oxide temperatures. However, given the questions regarding the significance of Fe-Ti oxide temperatures discussed above, we argue that the geological significance of these correlations is questionable. Furthermore, as initially pointed out by Gualda et al. (2012) and further developed by Gualda and Ghiorso (2013a), the original mineral compositions of Hildreth (1979) and the glass inclusion compositions of Wallace et al. (1999) both show bimodal distributions, in contrast with what would be expected for a compositionally stratified magma body. Gualda and Ghiorso (2013a) conclude that the bimodality suggests the existence of at least two chemically independent magma bodies. Evans et al. (2016) posit that the bimodality is the result of glass inclusions and crystal-core compositions that do not record the latest re-equilibration of late-erupted magmas with rejuvenated melt, which masks the evidence for a compositional continuum.

Our results here further support and expand upon the conclusions of Gualda and Ghiorso (2013a). We find three distinct compositional groups in terms of compositions of matrix glass. The lack of a continuum in compositions within matrix glass rules out the hypothesis of Evans et al. (2016) that the bimodality in compositions emphasized by Gualda et al. (2012) and Gualda and Ghiorso (2013a) results from the analysis of melt inclusions located in crystal interiors. Our data provide compelling evidence that a single stratified magma body did not exist, and—instead—discrete magma bodies characterized the pre-eruptive Bishop Tuff system. This is further reinforced by the fact that the compositional groups correlate well with stratigraphic position and geographic distribution, which also stands as strong evidence of discrete magma bodies. As such, we expand on the concept advanced by Gualda and Ghiorso (2013a) and suggest that there were three chemically independent main magma bodies that fed the Bishop Tuff eruption.

Interestingly, Chamberlain et al. (2015) generally accept the interpretation of Gualda and Ghiorso (2013a) that early- and late-erupted magmas were displaced laterally from each other, differing from Gualda and Ghiorso (2013a) only on the depth at which these magmas were located. Chamberlain et al. (2015) further emphasize that minor units may bridge the compositional gap between the main compositional types present in the deposit. This is a relatively minor issue and probably more a point of emphasis than a significant disagreement. We conclude that the Bishop Tuff eruption tapped three main parcels of magma that were laterally juxtaposed. Hildreth (1979) emphasizes that feldspar compositions show very little variation within a given pumice clast, and use that as evidence to suggest a lack of mixing in the pre-eruptive magma body—however, it is difficult to explain the lack of convective mixing in a magma body of the dimensions and with the characteristics of those inferred for a single Bishop Tuff magma body. In contrast, the existence of individual magma bodies helps explain the lack of mixing between different magma types, but allows for convective mixing in individual magma bodies. We accept that other, much smaller parcels of magma might have been present in the crust at the time and that they could have been involved in the eruption—but that does not change the essence of our model, which reveals that three independent, volumetrically dominant bodies of magma contributed to the Bishop Tuff supereruption.

Importantly, the distribution of these magma bodies can be reconciled with the detailed stratigraphy and inferred vent distribution developed by Wilson and Hildreth (1997) (see also Hildreth and Mahood, 1986). The earliest deposits erupted from a vent limited to the southern part of the caldera (Figure 1), which led to preservation of early-erupted deposits only to the South and East of the caldera and to the south of the Glass Mountain volcanic edifice. The vent location suggests that the magma body that led to eruption of early-erupted units was located to the south of the caldera (orange in Figure 9). Following this initial period of primarily fall deposition, vents opened in an unzipping pattern in two parts of the caldera. We infer that the late-erupted deposits to the east and south (what we call East-sector) erupted from one such set of vents, along the southeastern rim of the caldera, consistent with this magma body being located on the eastern part of the caldera (gray in Figure 9).

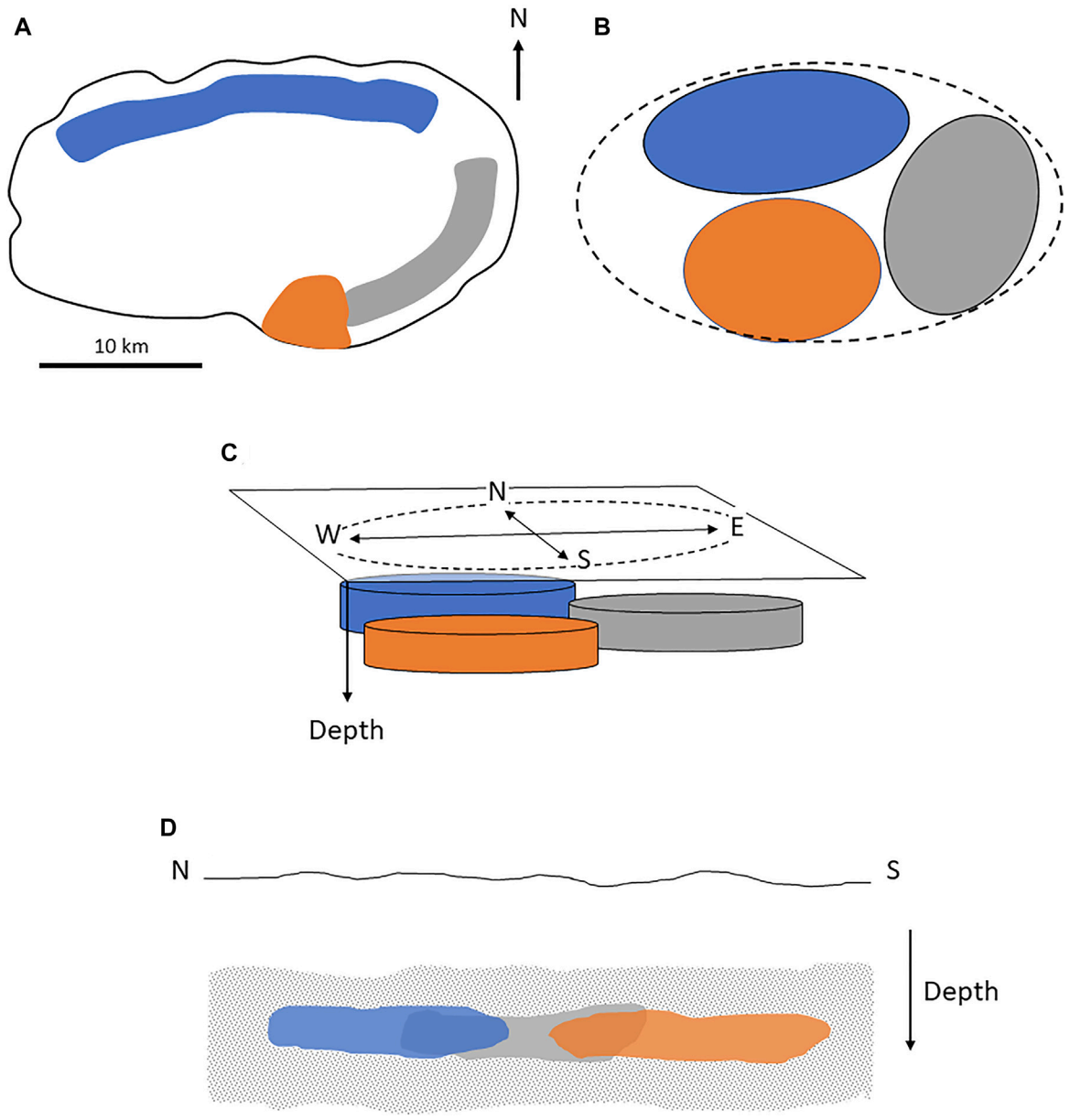

FIGURE 9
Inferred distribution of vents and magmas in the Bishop Tuff magmatic system. **(A)** Simplified map of the distribution of vents, modified from Figure 1. **(B)** Inferred distribution of magma bodies, in plan view. **(C)** Three dimensional schematic of putative distribution of magmas in the Bishop Tuff magmatic system. **(D)** Schematic N-S view of the distribution of magmas; view is from the West, with gray body behind blue and orange ones. We infer the presence of three distinct magma bodies, based on the compositional diversity seen in the matrix glass compositions; all magmas appear at approximately the same depth, and their locations in plan view can be correlated with the distribution of vents from which they erupted.

The other set of vents, along the northern margin of the caldera, led to the deposition of the North-sector late-erupted units, suggesting that the magma body that fed this part of the eruption was located on the northern portions of the caldera (blue in Figure 9).

The architecture of supereruption-feeding magmatic systems

The work of Hildreth (1979) suggests a clear picture for the architecture of magma bodies that feed supereruptions, in which a single, giant, thermally and compositionally stratified magma body fed a supereruption in a continuous event. This model for the Bishop Tuff magma system (which Gualda and Ghiorso, 2013a referred to as the "Standard Model") proved highly influential over the last 4 decades, giving the Bishop Tuff a special status as the archetypal example of the architecture of supereruption-feeding magmatic systems.

The model we infer here (an extension of the one proposed by Gualda and Ghiorso, 2013a) is quite distinct from the Standard Model, suggesting that three main magma bodies—and possibly a number of smaller ones—coexisted in the crust at the time of eruption and were tapped to feed a supereruption. In other words, we infer a patchwork of more or less isolated, laterally juxtaposed bodies of eruptible magma that occupied the same structural level in the crust. This is a picture similar to what has emerged from other studies of very large and supereruptions, including the Kidnappers Ignimbrite (Cooper et al., 2012) and the paired Ohakuri-Mamaku eruption (Gravley et al., 2007; Bégué et al., 2014a) in the Taupo Volcanic Zone, New Zealand; the Huckleberry Ridge Tuff (Swallow et al., 2018), United States ; and the Young Toba Tuff (Pearce et al., 2019), Indonesia. The mounting evidence suggests that very large to supereruptions are the result of a complex patchwork of magma bodies that coexist for brief periods of time (Gualda et al., 2012; Gualda and Sutton, 2016) and can be mobilized over days to months (Wilson and Hildreth, 1997; Wilson et al., 2006; Gualda and Sutton, 2016) to generate these catastrophic events.

Interestingly, the ephemeral presence of several large magma bodies may help resolve some of the conundrums associated with the dynamics of construction and eruption of very large to giant bodies of magma in the shallow crust. For instance, Jellinek and DePaolo (2003) argue that it may be difficult to generate enough overpressure in bodies of magma larger than 100 km^3 to promote eruption because the crust can accommodate pressurization by viscous flow. If the crust is characterized by a patchwork of contemporaneous magma bodies, however, it may be possible to trigger eruption of one these magma bodies, which could change the stress field in the nearby crust and ultimately lead to eruption of other nearby magma bodies in close succession. While this conceptual model is somewhat speculative at this point, it is interesting to note that Tramontano et al. (2017) suggest that the early-erupted Bishop Tuff was more likely primed to erupt—by exsolution of volatiles due to crystallization—compared to magmas that formed the late-erupted Bishop Tuff. We therefore suggest that the early-erupted magmas erupted during Plinian events from a vent near the south of the caldera, which then triggered a cascade of events that destabilized the crust and led to progressive eruption of the other magma bodies present at the time.

Another puzzling characteristic of supereruption-forming magmatic systems is the relatively extensive timescales over which eruptions seem to occur in some systems. Wilson et al. (2006) argue that the Oruanui eruption (Taupo Volcanic Zone, NZ) "effectively emptied [its] holding chamber", completely erupting a diverse suite of magmas, over timescales of several months to a year. If a complex patchwork of magma bodies is present in the shallow crust, and these magma bodies erupt successively due to the progressive destabilization of the crust, it becomes easier to explain why some supereruptions appear to have happened largely uninterrupted and only lasted days to weeks (e.g., Bishop Tuff; Wilson and Hildreth, 1997) while others preserve evidence of significant hiatuses, with total durations that could span several months to years (e.g., Oruanui Tuff; Wilson et al., 2006).

Further, Wilson et al. (2006) conclude that the eruptible magma that fed the Oruanui eruption was "physically separated from any crystal-richer root zone". This is consistent with the record from the Bishop Tuff, which entirely lacks remnants of the mush from which these magmas have separated (Hildreth, 1979; Wilson and Hildreth, 1997; Hildreth and Wilson, 2007). Similarly, the Taupo Volcanic Zone flare-up (Gravley et al., 2016) preserves evidence of separation between mush and eruptible magma based on storage and extraction pressures derived from rhyolite-MELTS calculations (Gualda et al., 2019). The existence of multiple magma bodies in these systems could suggest that 1) magmas are relatively mobile in the shallow crust; and 2) the presence of other magma bodies may facilitate magma stalling at certain structural crustal levels. The controls on magma mobility and on levels in which they accumulate are topics that deserve more detailed scrutiny.

Finally, it is interesting to note that other systems do not fit this model as naturally. The Peach Spring Tuff, SW United States (Young and Brennan, 1974; Buesch and Valentine, 1986; Glazner et al., 1986; Nielson et al., 1990; Ferguson et al., 2013) much more closely fits the Standard Model of Hildreth (1979), with no evidence to date (Pamukcu et al., 2013; Foley et al., 2020) suggesting multiple discrete bodies of high-silica rhyolite existed (evidently, further work could change this scenario). In fact, the picture emerging from the Peach Spring Tuff also fits more naturally the conventional scenario proposed for the Mush Model (Bachmann et al., 2002; Bachmann and Bergantz,

2004, 2008a, 2008b), in which high-silica rhyolites are extracted *in situ* from and coexist with a crystal-rich granodioritic mush. This should serve as a note of caution in any attempt to find a single model that could be applied to all supereruption-forming systems.

Conclusion

In this study, we use matrix-glass major and trace-element compositions to determine pre-eruptive crystallization temperatures (from zircon-saturation geothermometry) and pressures (using rhyolite-MELTS geobarometry) relevant for magmas that fed the Bishop Tuff supereruption. We demonstrate that pumice from three different stratigraphic groups comprise 3 separate compositional groups, suggesting the existence of three discrete bodies of magma. The distribution of crystallization pressures and temperatures is very similar for all three groups, suggesting lateral juxtaposition of these magma bodies. In this sense, our results are entirely inconsistent with the idea of a vertically stratified magma body. Previously determined distribution of the vents for each stratigraphic group allows us to infer the geographic distribution of these magma bodies. Our results add to growing evidence that supereruptions are often fed from a patchwork of large magma bodies rather than by a single giant magma body, which could help explain aspects related to the mechanics of the crust, mechanisms of triggering, as well as timescales of evolution and eruption of supereruption-forming magmatic systems.

Data availability statement

The original contributions presented in the study are included in the article/Supplementary Material, further inquiries can be directed to the corresponding author.

Author contributions

GG and MG conceived the study. AH, MA, and RB performed the analytical work. GG did most of the analysis, with input from MG. All authors contributed to the final draft.

Funding

This work was funded primarily using Vanderbilt University internal funds.

Acknowledgments

Gualda's work on the Bishop Tuff started under the guidance of the late Fred Anderson (Alfred T. Anderson Jr); Fred was an incredible mentor and his presence and thoughtful comments are sorely missed. Ghiorso was "in the room" when Hildreth and Carmichael first "discussed" the Bishop magma body—the issues pondered then still haunt him today. While debate regarding the origin, evolution, and eruption of the Bishop Tuff has been rather sanguine, it has provided important motivation for more detailed studies of the petrology and volcanology of supereruption-forming systems—we do not expect this will be the last word on the issues addressed here, but we hope they will be a step towards better understanding rhyolitic magmatism.

Conflict of interest

The authors declare that the research was conducted in the absence of any commercial or financial relationships that could be construed as a potential conflict of interest.

Publisher's note

Supplementary material

The Supplementary Material for this article can be found online at: https://www.frontiersin.org/articles/10.3389/feart.2022.798387/full#supplementary-material

References

Andersen, N. L., Jicha, B. R., Singer, B. S., and Hildreth, W. (2017). Incremental heating of Bishop Tuff sanidine reveals preeruptive radiogenic Ar and rapid remobilization from cold storage. *Proc. Natl. Acad. Sci. U. S. A.* 114, 12407–12412. doi:10.1073/pnas.1709581114

Anderson, A. T., Davis, A. M., and Lu, F. Q. (2000). Evolution of Bishop Tuff rhyolitic magma based on melt and magnetite inclusions and zoned phenocrysts. *J. Petrology* 41, 449–473. doi:10.1093/petrology/41.3.449

Annen, C., Blundy, J. D., Leuthold, J., and Sparks, R. S. J. (2015). Construction and evolution of igneous bodies: Towards an integrated perspective of crustal magmatism. *Lithos* 230, 206–221. doi:10.1016/j.lithos.2015.05.008

Bachmann, O., and Bergantz, G. W. (2004). On the origin of crystal-poor rhyolites: Extracted from batholithic crystal mushes. *J. Petrology* 45, 1565–1582. doi:10.1093/petrology/egh019

Bachmann, O., and Bergantz, G. W. (2008a). Rhyolites and their source mushes across tectonic settings. *J. Petrology* 49, 2277–2285. doi:10.1093/petrology/egn068

Bachmann, O., and Bergantz, G. W. (2008b). The magma reservoirs that feed supereruptions. *Elements* 4, 17–21. doi:10.2113/gselements.4.1.17

Bachmann, O., Dungan, M. A., and Lipman, P. W. (2002). The Fish Canyon magma body, San Juan volcanic field, Colorado: Rejuvenation and eruption of an upper-crustal batholith. *J. Petrology* 43, 1469–1503. doi:10.1093/petrology/43.8.1469

Bailey, R. A., Dalrymple, G. B., and Lanphere, M. A. (1976). Volcanism, structure, and geochronology of long-Valley caldera, mono-county, California. *J. Geophys. Res.* 81, 725–744. doi:10.1029/jb081i005p00725

Bégué, F., Deering, C. D., Gravley, D. M., Kennedy, B. M., Chambefort, I., Gualda, G. A. R., et al. (2014a). Extraction, storage and eruption of multiple isolated magma batches in the paired mamaku and Ohakuri eruption, Taupo volcanic zone, New Zealand. *J. Petrology* 55, 1653–1684. doi:10.1093/petrology/egu038

Bégué, F., Gualda, G. A. R., Ghiorso, M. S., Pamukcu, A. S., Kennedy, B. M., Gravley, D. M., et al. (2014b). Phase-equilibrium geobarometers for silicic rocks based on rhyolite-MELTS. Part 2: application to Taupo volcanic zone rhyolites. *Contrib. Mineral. Pet.* 168, 1082. doi:10.1007/s00410-014-1082-7

Bindeman, I. N., and Valley, J. W. (2002). Oxygen isotope study of the Long Valley magma system, California: isotope thermometry and convection in large silicic magma bodies. *Contrib. Mineral. Pet.* 144, 185–205. doi:10.1007/s00410-002-0371-8

Blundy, J., and Cashman, K. (2001). Ascent-driven crystallisation of dacite magmas at mount st helens, 1980-1986. *Contrib. Mineral. Pet.* 140, 631–650. doi:10.1007/s004100000219

Boehnke, P., Watson, E. B., Trail, D., Harrison, T. M., and Schmitt, A. K. (2013). Zircon saturation re-revisited. *Chem. Geol.* 351, 324–334. doi:10.1016/j.chemgeo.2013.05.028

Buesch, D. C., and Valentine, G. A. (1986). "Peach Springs Tuff and volcanic stratigraphy of the southern Cerbat Mountains, Kingman, Arizona," in Cenozoic stratigraphy, structure and mineralization in the Mojave Desert, Guidebook and Volume, Prepared for the 82nd Annual Meeting of the Cordilleran Section of the Geological Society America, Los Angeles, Calif., March 25-28, 1986, Field Trip Numbers 5 and 6: Los Angeles, California State University, p. 7–13.

Cashman, K. V., and Giordano, G. (2014). Calderas and magma reservoirs. *J. Volcanol. Geotherm. Res.* 288, 28–45. doi:10.1016/j.jvolgeores.2014.09.007

Cashman, K. V., Sparks, R. S. J., and Blundy, J. D. (2017). Vertically extensive and unstable magmatic systems: A unified view of igneous processes. *Science* 355, eaag3055. doi:10.1126/science.aag3055

Chamberlain, K., Morgan, D., and Wilson, C. (2014a). Timescales of mixing and mobilisation in the Bishop Tuff magma body: perspectives from diffusion chronometry. *Contrib. Mineral. Pet.* 168, 1034. doi:10.1007/s00410-014-1034-2

Chamberlain, K., Wilson, C., Wallace, P., and Millet, M. (2015). Micro-analytical perspectives on the Bishop Tuff and its magma chamber. *J. Petrology* 56, 605–640. doi:10.1093/petrology/egv012

Chamberlain, K., Wilson, C., Wooden, J., Charlier, B., and Ireland, T. (2014b). New perspectives on the Bishop Tuff from zircon textures, ages and trace elements. *J. Petrology* 55, 395–426. doi:10.1093/petrology/egt072

Cooper, G. F., Wilson, C. J. N., Millet, M.-A., Baker, J. A., and Smith, E. G. C. (2012). Systematic tapping of independent magma chambers during the 1 Ma Kidnappers supereruption. *Earth Planet. Sci. Lett.* 313, 23–33. doi:10.1016/j.epsl.2011.11.006

Evans, B. W., and Bachmann, O. (2013). Implications of equilibrium and disequilibrium among crystal phases in the Bishop Tuff. *Am. Mineralogist* 98, 271–274. doi:10.2138/am.2013.4280

Evans, B. W., Hildreth, W., Bachmann, O., and Scaillet, B. (2016). In defense of magnetite-ilmenite thermometry in the Bishop Tuff and its implication for gradients in silicic magma reservoirs. *Am. Mineralogist* 101, 469–482. doi:10.2138/am-2016-5367

Ferguson, C. A., McIntosh, W. C., and Miller, C. F. (2013). Silver creek caldera-the tectonically dismembered source of the Peach spring Tuff. *Geol.* 41, 3–6. doi:10.1130/g33551.1

Foley, M. L., Miller, C. F., and Gualda, G. A. R. (2020). Architecture of a super-sized magma chamber and remobilization of its basal cumulate (Peach Spring Tuff, USA). *J. Petrology* 61. doi:10.1093/petrology/egaa020

Gardner, J. E., Befus, K. S., Gualda, G. A. R., and Ghiorso, M. S. (2014). Experimental constraints on rhyolite-MELTS and the Late Bishop Tuff magma body. *Contrib. Mineral. Pet.* 168, 1051. doi:10.1007/s00410-014-1051-1

Ghiorso, M. S., and Evans, B. W. (2008). Thermodynamics of rhombohedral oxide solid solutions and a revision of the Fe-Ti two-oxide geothermometer and oxygen-barometer. *Am. J. Sci.* 308, 957–1039. doi:10.2475/09.2008.01

Ghiorso, M. S., and Gualda, G. A. R. (2013). A method for estimating the activity of titania in magmatic liquids from the compositions of coexisting rhombohedral and cubic iron-titanium oxides. *Contrib. Mineral. Pet.* 165, 73–81. doi:10.1007/s00410-012-0792-y

Ghiorso, M. S., and Gualda, G. A. R. (2015). An H2O-CO2 mixed fluid saturation model compatible with rhyolite-MELTS. *Contrib. Mineral. Pet.* 169, 53. doi:10.1007/s00410-015-1141-8

Glazner, A. F., Nielson, J. E., Howard, K. A., and Miller, D. M. (1986). Correlation of the Peach springs Tuff, a large-volume miocene ignimbrite sheet in California and Arizona. *Geol.* 14, 840–843. doi:10.1130/0091-7613(1986)14<840:cotpst>2.0.co;2

Gravley, D. M., Deering, C. D., Leonard, G. S., and Rowland, J. V. (2016). Ignimbrite flare-ups and their drivers: A New Zealand perspective. *Earth-Science Rev.* 162, 65–82. doi:10.1016/j.earscirev.2016.09.007

Gravley, D. M., Wilson, C. J. N., Leonard, G. S., and Cole, J. W. (2007). Double trouble: Paired ignimbrite eruptions and collateral subsidence in the Taupo Volcanic Zone, New Zealand. *Geol. Soc. Am. Bull.* 119, 18–30. doi:10.1130/b25924.1

Griffin, W. L., Powell, W. J., Pearson, N. J., and O'Reilly, S. Y. (2008). "GLITTER: Data reduction software for laser ablation ICP-MS," in *Laser ablation-ICP-MS in the Earth Sciences*, 204–207.

Gualda, G. A. R., and Anderson, A. T. (2007). Magnetite scavenging and the buoyancy of bubbles in magmas. Part 1: Discovery of a pre-eruptive bubble in Bishop rhyolite. *Contrib. Mineral. Pet.* 153, 733–742. doi:10.1007/s00410-006-0173-5

Gualda, G. A. R., Cook, D. L., Chopra, R., Qin, L. P., Anderson, A. T., and Rivers, M. (2004). Fragmentation, nucleation and migration of crystals and bubbles in the Bishop Tuff rhyolitic magma. *Earth Environ. Sci. Trans. R. Soc. Edinb.* 95, 375–390. doi:10.1017/s0263593300001139

Gualda, G. A. R. (2006). Crystal size distributions derived from 3D datasets: Sample size versus uncertainties. *J. Petrology* 47, 1245–1254. doi:10.1093/petrology/egl010

Gualda, G. A. R., Ghiorso, M. S., Lemons, R. V., and Carley, T. L. (2012). Rhyolite-MELTS: A modified calibration of MELTS optimized for silica-rich, fluid-bearing magmatic systems. *J. Petrology* 53, 875–890. doi:10.1093/petrology/egr080

Gualda, G. A. R., and Ghiorso, M. S. (2013b). Low-pressure origin of high-silica rhyolites and granites. *J. Geol.* 121, 537–545. doi:10.1086/671395

Gualda, G. A. R., and Ghiorso, M. S. (2007). Magnetite scavenging and the buoyancy of bubbles in magmas. Part 2: Energetics of crystal-bubble attachment in magmas. *Contrib. Mineral. Pet.* 154, 479–490. doi:10.1007/s00410-007-0206-8

Gualda, G. A. R., and Ghiorso, M. S. (2014). Phase-equilibrium geobarometers for silicic rocks based on rhyolite-MELTS. Part 1: Principles, procedures, and evaluation of the method. *Contrib. Mineral. Pet.* 168, 1033. doi:10.1007/s00410-014-1033-3

Gualda, G. A. R., and Ghiorso, M. S. (2013a). The Bishop Tuff giant magma body: an alternative to the standard model. *Contrib. Mineral. Pet.* 166, 755–775. doi:10.1007/s00410-013-0901-6

Gualda, G. A. R., Gravley, D. M., Deering, C. D., and Ghiorso, M. S. (2019). Magma extraction pressures and the architecture of volcanic plumbing systems. *Earth Planet. Sci. Lett.* 522, 118–124. doi:10.1016/j.epsl.2019.06.020

Gualda, G. A. R., and Rivers, M. (2006). Quantitative 3D petrography using X-ray tomography: Application to Bishop Tuff pumice clasts. *J. Volcanol. Geotherm. Res.* 154, 48–62. doi:10.1016/j.jvolgeores.2005.09.019

Gualda, G. A. R., and Sutton, S. R. (2016). The year leading to a supereruption. *Plos One* 11, e0159200. doi:10.1371/journal.pone.0159200

Halliday, A. N., Fallick, A. E., Hutchinson, J., and Hildreth, W. (1984). A Nd, Sr and O isotopic investigation into the causes of chemical and isotopic zonation in the Bishop-Tuff, California. *Earth Planet. Sci. Lett.* 68, 379–391. doi:10.1016/0012-821x(84)90123-7

Hanchar, J. M., and Watson, E. B. (2003). Zircon saturation thermometry. *Rev. Mineral. Geochem.* 53, 89–112. doi:10.2113/0530089

Hildreth, W. (1979). The Bishop Tuff: Evidence for the origin of compositional zonation in silicic magma chambers. *Geol. Soc. Am. Sp. Paper* 180, 43–75. doi:10.1130/SPE180-p43

Hildreth, W., and Mahood, G. A. (1986). Ring-fracture eruption of the Bishop Tuff. *Geol. Soc. Am. Bull.* 97, 396–403. doi:10.1130/0016-7606(1986)97<396:reotbt>2.0.co;2

Hildreth, W. (2004). Volcanological perspectives on Long Valley, mammoth mountain, and mono craters: Several contiguous but discrete systems. *J. Volcanol. Geotherm. Res.* 136, 169–198. doi:10.1016/j.jvolgeores.2004.05.019

Hildreth, W., and Wilson, C. J. N. (2007). Compositional zoning of the Bishop Tuff. *J. Petrology* 48, 951–999. doi:10.1093/petrology/egm007

Jellinek, A. M., and DePaolo, D. J. (2003). A model for the origin of large silicic magma chambers: precursors of caldera-forming eruptions. *Bull. Volcanol.* 65, 363–381. doi:10.1007/s00445-003-0277-y

Jolles, J. S. R., and Lange, R. A. (2019). High-resolution Fe-Ti oxide thermometry applied to single-clast pumices from the Bishop Tuff: a re-examination of compositional variations in phenocryst phases with temperature. *Contrib. Mineral. Pet.* 174, 70. doi:10.1007/s00410-019-1597-z

Klimm, K., Holtz, F., and King, P. L. (2008). Fractionation vs. magma mixing in the wangrah suite A-type granites, lachlan fold belt, Australia: Experimental constraints. *Lithos* 102, 415–434. doi:10.1016/j.lithos.2007.07.018

Miller, C. F., McDowell, S. M., and Mapes, R. W. (2003). Hot and cold granites? Implications of zircon saturation temperatures and preservation of inheritance. *Geol.* 31, 529. doi:10.1130/0091-7613(2003)031<0529:hacgio>2.0.co;2

Nielson, J. E., Lux, D. R., Dalrymple, G. B., and Glazner, A. F. (1990). Age of the Peach springs Tuff, southeastern California and western Arizona. *J. Geophys. Res.* 95, 571. doi:10.1029/jb095ib01p00571

Pamukcu, A. S., Carley, T. L., Gualda, G. A. R., Miller, C. F., and Ferguson, C. A. (2013). The evolution of the Peach spring giant magma body: Evidence from accessory mineral textures and compositions, bulk pumice and glass geochemistry, and rhyolite-MELTS modeling. *J. Petrology* 54, 1109–1148. doi:10.1093/petrology/egt007

Pamukcu, A. S., Ghiorso, M. S., and Gualda, G. A. R. (2016). High-Ti, bright-CL rims in volcanic quartz: a result of very rapid growth. *Contrib. Mineral. Pet.* 171, 105. doi:10.1007/s00410-016-1317-x

Pamukcu, A. S., Gualda, G. A. R., and Anderson, A. T., Jr. (2012). Crystallization stages of the Bishop Tuff magma body recorded in crystal textures in pumice clasts. *J. Petrology* 53, 589–609. doi:10.1093/petrology/egr072

Pamukcu, A. S., Gualda, G. A. R., Begue, F., and Gravley, D. M. (2015a). Melt inclusion shapes: Timekeepers of short-lived giant magma bodies. *Geol.* 43, 947–950. doi:10.1130/g37021.1

Pamukcu, A. S., Gualda, G. A. R., Ghiorso, M. S., Miller, C. F., and McCracken, R. G. (2015b). Phase-equilibrium geobarometers for silicic rocks based on rhyolite-MELTS-Part 3: Application to the Peach Spring Tuff (Arizona-California-Nevada, USA). *Contrib. Mineral. Pet.* 169, 33. doi:10.1007/s00410-015-1122-y

Pamukcu, A. S., Gualda, G. A. R., and Gravley, D. M. (2021). Rhyolite-MELTS and the storage and extraction of large-volume crystal-poor rhyolitic melts at the taupō volcanic center: a reply to Wilson et al. (2021). *Contrib. Mineral. Pet.* 176, 82. doi:10.1007/s00410-021-01840-2

Pearce, N. J. G., Westgate, J. A., Gualda, G. A. R., Gatti, E., and Muhammad, R. F. (2019). Tephra glass chemistry provides storage and discharge details of five magma reservoirs which fed the 75 ka Youngest Toba Tuff eruption, northern Sumatra. *J. Quat. Sci.* 35, 256–271. doi:10.1002/jqs.3149

Peppard, B. T., Steele, I. M., Davis, A. M., Wallace, P. J., and Anderson, A. T. (2001). Zoned quartz phenocrysts from the rhyolitic Bishop Tuff. *Am. Mineralogist* 86, 1034–1052. doi:10.2138/am-2001-8-910

Pitcher, B. W., Gualda, G. A. R., and Hasegawa, T. (2021). Repetitive duality of rhyolite compositions, timescales, and storage and extraction conditions for pleistocene caldera-forming eruptions, hokkaido, Japan. *J. Petrology* 62, egaa106. doi:10.1093/petrology/egaa106

Reid, M. R., and Coath, C. D. (2000). *In situ* U-Pb ages of zircons from the Bishop Tuff: No evidence for long crystal residence times. *Geol.* 28, 443–446. doi:10.1130/0091-7613(2000)028<0443:isupao>2.3.co;2

Reid, M. R., Vazquez, J. A., and Schmitt, A. K. (2011). Zircon-scale insights into the history of a supervolcano, Bishop Tuff, Long Valley, California, with implications for the Ti-in-zircon geothermometer. *Contrib. Mineral. Pet.* 161, 293–311. doi:10.1007/s00410-010-0532-0

Roberge, J., Wallace, P. J., and Kent, A. J. R. (2013). Magmatic processes in the Bishop Tuff rhyolitic magma based on trace elements in melt inclusions and pumice matrix glass. *Contrib. Mineral. Pet.* 165, 237–257. doi:10.1007/s00410-012-0807-8

Sheridan, M. F. (1965). *The mineralogy and petrology of the Bishop Tuff.* PhD thesis. Palo Alto, CA: Stanford University.

Simon, J. I., and Reid, M. R. (2005). The pace of rhyolite differentiation and storage in an "archetypical" silicic magma system, Long Valley, California. *Earth Planet. Sci. Lett.* 235, 123–140. doi:10.1016/j.epsl.2005.03.013

Swallow, E. J., Wilson, C. J. N., Myers, M. L., Wallace, P. J., Collins, K. S., and Smith, E. G. C. (2018). Evacuation of multiple magma bodies and the onset of caldera collapse in a supereruption, captured in glass and mineral compositions. *Contrib. Mineral. Pet.* 173, 33. doi:10.1007/s00410-018-1459-0

Tomiya, A., Miyagi, I., Saito, G., and Geshi, N. (2013). Short time scales of magma-mixing processes prior to the 2011 eruption of Shinmoedake volcano, Kirishima volcanic group, Japan. *Bull. Volcanol.* 75, 750. doi:10.1007/s00445-013-0750-1

Tramontano, S., Gualda, G. A. R., and Ghiorso, M. S. (2017). Internal triggering of volcanic eruptions: tracking overpressure regimes for giant magma bodies. *Earth Planet. Sci. Lett.* 472, 142–151. doi:10.1016/j.epsl.2017.05.014

Van Orman, J. A., and Crispin, K. L. (2010). Diffusion in oxides. *Rev. Mineralogy Geochem.* 72, 757–825. doi:10.2138/rmg.2010.72.17

Wallace, P. J., Anderson, A. T., and Davis, A. M. (1999). Gradients in H2O, CO2, and exsolved gas in a large-volume silicic magma system: Interpreting the record preserved in melt inclusions from the Bishop Tuff. *J. Geophys. Res.* 104, 20097–20122. doi:10.1029/1999jb900207

Wallace, P. J., Anderson, A. T., and Davis, A. M. (1995). Quantification of pre-eruptive exsolved gas contents in silicic magmas. *Nature* 377, 612–616. doi:10.1038/377612a0

Wark, D. A., Hildreth, W., Spear, F. S., Cherniak, D. J., and Watson, E. B. (2007). Pre-eruption recharge of the Bishop magma system. *Geol.* 35, 235–238. doi:10.1130/g23316a.1

Watson, E. B., and Harrison, T. M. (1983). Zircon saturation revisited: temperature and composition effects in a variety of crustal magma types. *Earth Planet. Sci. Lett.* 64, 295–304. doi:10.1016/0012-821x(83)90211-x

Watson, E. B. (1979). Zircon saturation in felsic liquids: Experimental results and applications to trace-element geochemistry. *Contr. Mineral. Pet.* 70, 407–419. doi:10.1007/bf00371047

Wilson, C. J. N., Blake, S., Charlier, B. L. A., and Sutton, A. N. (2006). The 26.5 ka Oruanui eruption, Taupo volcano, New Zealand: Development, characteristics and evacuation of a large rhyolitic magma body. *J. Petrology* 47, 35–69. doi:10.1093/petrology/egi066

Wilson, C. J. N., and Hildreth, W. (1997). The Bishop Tuff: New insights from eruptive stratigraphy. *J. Geol.* 105, 407–440. doi:10.1086/515937

Young, R. A., and Brennan, W. J. (1974). Peach springs Tuff: Its bearing on structural evolution of the Colorado plateau and development of cenozoic drainage in mohave county, Arizona. *Geol. Soc. Am. Bull.* 85, 83–90. doi:10.1130/0016-7606(1974)85<83:pstibo>2.0.co;2